HHS Public Access

Author manuscript

Bioorg Chem. Author manuscript; available in PMC 2023 April 01.

Published in final edited form as:

Bioorg Chem. 2022 April ; 121: 105660. doi:10.1016/j.bioorg.2022.105660.

Chemical synthesis, biological activities and action on nuclear receptors of 20*S*(OH)D_3, 20*S*,25(OH)$_2D_3$, 20*S*,23*S*(OH)$_2D_3$ and 20*S*,23*R*(OH)$_2D_3$

Pawel Brzeminski[1,2,#], **Adrian Fabisiak**[1,2,#], **Radomir M. Slominski**[2,3], **Tae-Kang Kim**[2], **Zorica Janjetovic**[2], **Ewa Podgorska**[2], **Yuwei Song**[2,3], **Mohammad Saleem**[2], **Sivani B. Reddy**[2], **Shariq Qayyum**[2], **Yuhua Song**[4], **Robert C. Tuckey**[5], **Venkatram Atigadda**[2], **Anton M. Jetten**[6], **Rafal R. Sicinski**[1], **Chander Raman**[2], **Andrzej T. Slominski**[2,7,*]

[1]Department of Chemistry, University of Warsaw, Pasteura 1, 02-093 Warsaw, Poland

[2]Department of Dermatology, University of Alabama at Birmingham, Birmingham, AL 35294, USA

[3]Graduate Biomedical Sciences Program, University of Alabama at Birmingham, Birmingham, AL 35294, USA

[4]Department of Biomedical Engineering, University of Alabama at Birmingham, Birmingham, AL 35294, USA

[5]School of Molecular Sciences, The University of Western Australia, Perth, WA, Australia

[6]Cell Biology Section, National Institute of Environmental Health Sciences, National Institutes of Health, Research Triangle Park, NC 27709, USA

[7]Pathology Laboratory Service, Veteran Administration Medical Center at Birmingham, Birmingham, AL35294, USA.

Abstract

New and more efficient routes of chemical synthesis of vitamin D_3 (D_3) hydroxy (OH) metabolites, including 20*S*(OH)D_3, 20*S*,23*S*(OH)$_2D_3$ and 20*S*,25(OH)$_2D_3$, that are endogenously produced in the human body by CYP11A1, and of 20*S*,23*R*(OH)$_2D_3$ were established. The biological evaluation showed that these compounds exhibited similar properties to each other regarding inhibition of cell proliferation and induction of cell differentiation but with subtle and quantitative differences. They showed both overlapping and differential effects on T-cell immune activity. They also showed similar interactions with nuclear receptors with all secosteroids activating vitamin D and aryl hydrocarbon receptors in functional assays and also as indicated by molecular modeling. They functioned as substrates for CYP27B1 with enzymatic activity being the highest towards 20*S*,25(OH)$_2D_3$ and the lowest towards 20*S*(OH)D_3. In conclusion, defining new routes for large scale synthesis of endogenously produced D_3-hydroxy derivatives by

*corresponding author: Andrzej T. Slominski, aslominski@uabmc.edu.
#equal first authors, they contributed equally

pathways initiated by CYP11A1 opens an exciting era to analyze their common and differential activities *in vivo,* particularly on the immune system and inflammatory diseases.

Graphical Abstract

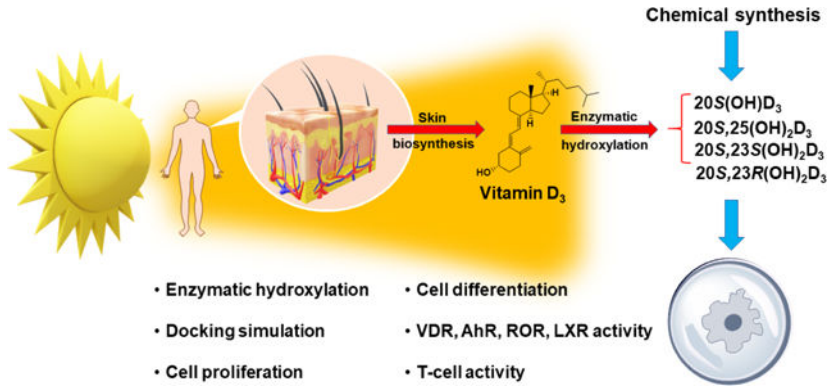

Introduction

Vitamin D_3 (**1**, Fig. 1) is formed from 7-dehydrocholesterol (7DHC) by the action of ultraviolet (UVB) radiation [1–4]. The electrocyclic B-ring opening generates previtamin D_3 which is converted to vitamin D_3 by a first-order thermal isomerization in the skin [1–3]. Vitamin D_3 is activated by hydroxylation at C-25 by CYP2R1 or CYP27A1 then at C1α by CYP27B1, to produce 1α,25$(OH)_2D_3$ (**2**) [4–7]. In addition to regulating calcium homeostasis, 1α,25$(OH)_2D_3$ has pleiotropic effects affecting almost all body functions through an interaction with vitamin D receptor (VDR) [4, 5, 8–16]. 1α,25$(OH)_2D_3$ regulates cell proliferation and differentiation, exhibits anticancer properties, regulates skin functions, inhibits adaptive immunity, and upregulates innate immune responses among other physiological functions [10, 17–21]. It is clinically used to treat autoimmune and inflammatory diseases, including various skin disorders [22–31]. However, toxic/calcemic effects of 1α,25$(OH)_2D_3$ at pharmacological doses constrains its use to treat autoimmune diseases and other pathological states [10, 12, 32–34].

New pathways of vitamin D_3 activation by CYP11A1 producing many hydroxy-derivatives have now been well characterized [7, 35]. The main sequence of the reactions starts with hydroxylation at C-20 to produce 20*S*$(OH)D_3$ (**3**) which is sequentially hydroxylated to 20*S*,23*S*$(OH)_2D_3$ (**4a**) and 17*R*,20*S*,23*S*$(OH)_3D_3$ (**5**) [35–37]. 20*S*$(OH)D_3$ can also be hydroxylated by CYP27A1, CYP24A1 and CYP2R1 to produce 20*S*,25$(OH)_2D_3$ (**6**), which is an excellent substrate for CYP27B1 [7]. These metabolites are produced *ex vivo* in skin cells, placenta and adrenal glands in a CYP11A1 dependent fashion [38, 39]. Some, including 20*S*$(OH)D_3$ and 1α,20*S*$(OH)_2D_3$, have been measured in the nM range in all human serum samples tested [40, 41] and 20*S*$(OH)D_3$ was recently detected in honey [42]. Thus, in addition to functioning as hormones in humans (see below), some of these secosteroids can be defined as natural products [43].

In vitro studies have demonstrated that 20*S*(OH)D_3 and 20*S*,23*S*$(OH)_2D_3$ show anti-proliferative, pro-differentiation, anticancer, photoprotective, anti-inflammatory and anti-fibrinogenic properties [44–52]. 20*S*,25$(OH)_2D_3$ has also been reported to exhibit anti-melanoma activity in cell culture [53]. Anti-fibrogenic, photoprotective and anti-melanoma properties for 20*S*(OH)D_3 were also demonstrated in *in vivo* models [50, 54, 55]. Of high clinical relevance is that CYP11A-derived 20*S*(OH)D_3 and 20*S*,23*S*$(OH)_2D_3$ are non-calcemic at doses that are highly toxic for 1α,25$(OH)_2D_3$ and 25(OH)D_3 [32, 50, 56]. The CYP11A1-derived secosteroids have been shown to mediate their effects by acting as biased agonists on the VDR [51, 57–59], inverse agonists on retinoic acid orphan receptors (ROR) α and γ [58, 60], and agonists on liver X receptors (LXRs) [61]. 20*S*(OH)D_3 and 20*S*,23*S*$(OH)_2D_3$ are also agonists for the aryl hydrocarbon receptor (AhR) [62].

To provide a robust source of key CYP11A1-derived secosteroids produced by pathways initiated by CYP11A1, and to enable better characterization of their biological activity, we describe new chemical routes for large scale synthesis of 20*S*(OH)D_3 (**3**), 20*S*,23*S*$(OH)_2D_3$ (**4a**), 20*S*,23*R*$(OH)_2D_3$ (**4b**) and 20*S*,25$(OH)_2D_3$ (**6**).

Results and Discussion

Chemical synthesis and confirmation of the structures

Continuing our studies related to vitamin D_3 derivatives we designed an efficient synthetic route for 20*S*(OH)D_3 and its 23- as well as 25-hydroxylated analogs 20*S*,23*S*$(OH)_2D_3$, 20*S*,23*R*$(OH)_2D_3$, 20*S*,25$(OH)_2D_3$. Convergent synthesis was used for the preparation of these target compounds where the key stage was a Wittig-Horner coupling of the corresponding Grundmann ketone (CD-ring fragment) with A-ring phosphine oxide. Starting from vitamin D_2 (**7**), the required building blocks **8** – **12** (Fig. 2) were prepared using a slight modification of literature procedures; the synthetic steps (Scheme S1), procedures and characterization of the compounds obtained are presented in Supporting Information.

The ketone **12** was treated with two different Grignard reagents [63, 64] providing diastereomerically pure 20*S*-diols **13** and **14** (Scheme 1). Secondary hydroxyl groups in **13** and **14** were efficiently oxidized to the corresponding ketones **15** and **16** with tetrapropylammonium perruthenate in the presence of *N*-methylmorpholine-*N*-oxide. Tertiary hydroxyls were then protected as TMS ethers providing CD-ring building blocks **17** and **18**. These hydrindanones were then coupled with the known A-ring phosphine oxide **9** [65] to furnish protected vitamin D_3 derivatives **19** and **20**. Their deprotection followed by RP-HPLC purification provided the target 20-hydroxy compounds **3** and **6** in good yields and high purity.

Methyl ketone **11** was then used for the preparation of desired 20*S*,23*S*$(OH)_2D_3$ as well as its epimer 20*S*,23*R*$(OH)_2D_3$ (Scheme 2). As a consequence of the steric effect of both 7a'-methyl group and 4'-OTES substituents, only the 3*S*-epimer **21** was isolated when the ketone **11** was treated with the nitrile anion, generated from acetonitrile and LDA. The analogous, highly stereoselective addition of Grignard reagents has been thoroughly studied by us previously [63,64]. The secondary hydroxyl group in **21** was deprotected and the

resulting hydrindanol **22** was subjected to the oxidation with TPAP/NMO leading to the ketone **23**. Protection of the tertiary hydroxyl group in this compound by its treatment with trimethylsilyl triflate provided the desired building block **24**. Wittig-Horner olefination was used as a coupling reaction of the hydrindanone **24** and phosphine oxide **9**. The formed nitrile **25**, possessing the vitamin D skeleton, was reduced with diisobutylaluminum hydride to the corresponding aldehyde **26**. In this compound elongation of the side chain was effected by its Grignard reaction with *i*-butyl magnesium chloride providing a mixture of diastereomeric alcohols **27a**,**b**. Finally, removal of silyl protecting groups and efficient separation by high-performance liquid chromatography (HPLC) provided the target epimeric (20*S*,23*S*)- and (20*S*,23*R*)-dihydroxylated vitamin D_3 compounds (**4a**,**b**).

The above scheme represents a significant improvement to the synthetic route for the preparation of 20*S*(OH)D_3 compared to the method described by Li et al [65]. The advantage of the synthesis reported here is the application of a different protecting group of the tertiary hydroxyl at C-20. Thus, the use of trimethylsilyl ether (OTMS), being significantly more labile than EOM ether, allowed us to obtain the final vitamin D compound with significantly increased (ca. fourfold) overall yield. Moreover, using analogous conditions, 20*S*,25$(OH)_2D_3$ has also been successfully prepared, representing another active metabolite of vitamin D_3, that so far has only been obtained enzymatically [66].

The synthesis of 23-hydroxylated derivatives presented above has also been significantly improved in comparison with the previously reported synthetic path [67] involving a series of linear transformations. The epimeric 20,23-dihydroxyvitamin D_3 metabolites were obtained in high yield, easily separated by HPLC and individual compounds were biologically evaluated. The synthetic strategy applied by us gave a marked (ca. 5 times) increase in the overall yield of the target secosteroids, avoiding the irradiation step used in past routes which limits the scale of the conversion of the 7-dehydrocholesterol analog to the corresponding secosteroid. Moreover, almost all steps are executed on the optically pure compounds; formation of C-23 stereoisomers takes place at the final stage of our synthesis.

Hydroxylation at C1α

All four chemically synthesized secosteroids were converted to their expected 1α-hydroxy derivatives by CYP27B1, and identified on the basis of previous studies on the enzymatically and/or chemically derived substrates [63, 66–68]. The rates varied dramatically with a high rate of 1α-hydroxylation being observed for 20*S*,25$(OH)_2D_3$ (Table 1), consistent with previous reports for this substrate produced enzymatically [66]. The naturally occurring diastereomer of 20,23$(OH)_2D_3$, the 20*S*,23*S*-isomer, was metabolized approximately twice as fast as the non-natural 20*S*,23*R*-isomer (Table 1), as noted in a previous study [67]. 20*S*(OH)D_3 was a relatively poorer substrate for CYP27B1 compared to 20*S*,25$(OH)_2D_3$ (Table 1), also consistent with a previous report [66]. In summary, the efficiency of metabolism of D_3 derivatives by CYP27B1 is as follows: 20*S*,25$(OH)_2D_3$ >> 20*S*,23*S*$(OH)_2D_3$ > 20*S*(OH)D_3 = 20*S*,23*R*$(OH)_2D_3$.

Regulation of cell proliferation and differentiation program

The anti-proliferative properties of 20*S*(OH)D_3 and 20*S*,23(OH)$_2D_3$ [44, 48–50, 52, 55, 56, 69–72] and to some degree of 20*S*,25(OH)$_2D_3$ [53, 58] are well established. We tested the capabilities of the newly synthesized secosteroids to inhibit proliferation and found that 20*S*,25(OH)$_2D_3$ inhibits fibroblast and keratinocyte proliferation in similar manner to its precursor, 20*S*(OH)D_3 (Fig. 3). Similar effects were also observed for both 20*S*,23(OH)$_2D_3$ isomers (Fig. 3), which is consistent with previously reported data [67]. Again, analysis of human keratinocytes showed that 20*S*,25(OH)$_2D_3$ was slightly better at inducing gene expression of involucrin, CK10, and filaggrin, indicative of keratinocyte differentiation, compared to 20*S*(OH)D_3 (Fig. 4A) with 20*S*,23*R*(OH)$_2D_3$ and 20*S*,25(OH)$_2D_3$ showing similar effects on the expression of these genes (Fig. 4B). At the protein level, all compounds including 20*S*(OH)D_3, 20*S*,23*S*(OH)$_2D_3$, 20*S*,23*R*(OH)$_2D_3$ and 20*S*,25(OH)$_2D_3$ showed similar net biological effects in increasing the levels of involucrin, CK10, CK14, and catalase (Fig. 4C). These results are consistent with previously published pro-differentiation properties of 20*S*(OH)D_3 and 20*S*,23*S*(OH)$_2D_3$ [32, 45, 48, 49, 69, 70, 73], which we now extend to include 20*S*,25(OH)$_2D_3$ and 20S,23*R*(OH)$_2D_3$.

Nuclear receptor signaling

To better define the properties of the newly synthesized secosteroids, we tested their activities on the VDR, AhR and LXR by performing functional assays which were further validated by qPCR of downstream enzymes (Fig. 5) and molecular modeling (Table 2 and Fig. 6). Binding affinities of top-scored docking complexes of vitamin D_3 hydroxy derivatives with VDR, AhR, LXRs (LXRα, LXRβ) and RORs (RORα, RORγ) from molecular docking are presented in Table 2, known ligands for each receptor were used as controls. 20*S*(OH)D_3, 20*S*,25(OH)$_2D_3$, 20*S*,23*S*(OH)$_2D_3$ and 20*S*,23*R*(OH)$_2D_3$ have favorable energies for binding to the ligand binding domain of VDR, AhR, LXRs (LXRα, LXRβ) and RORs (RORα, RORγ), and are comparable to the binding energies of known ligands for each receptor, including 1α,25(OH)$_2D_3$.

All of the newly-synthesised compounds induced VDR translocation to the nucleus (Fig. 5A) in a manner similar to that reported previously for some of these secosteroids [57, 74]. *CYP24A1* is a downstream target of the activated VDR and we observed that 20*S*,25(OH)$_2D_3$ caused much greater stimulation of *CYP24A1* expression than 20*S*(OH)D_3. There was no significant difference in the expression of *CYP24A1* caused by 20*S*,23*S*(OH)$_2D_3$ and 20*S*,23*R*(OH)$_2D_3$ but both of these caused significantly less expression than 1α,25(OH)$_2D_3$ (Fig. 5C). The results of these assays are supported by molecular docking results of these secosteroids with the VDR (Table 2 and Supplemental S72). 20*S*(OH)D_3, 20*S*,25(OH)$_2D_3$, 20*S*,23*S*(OH)$_2D_3$ and 20*S*,23*R*(OH)$_2D_3$ all have favorable to binding energies for interaction with VDR (Table 2) and bind to the same LBD of VDR (Supplemental S72).

In summary, these data and analyses are consistent with our previous studies on the VDR which showed that 20*S*(OH)D_3 and 20*S*,23(OH)$_2D_3$ act on the genomic site of the VDR with lower efficiency than their 1α-hydroxy derivatives, as a consequence of their different interactions with amino acids of the LBD [48, 57, 59, 67, 74]. The better efficiency

of 20*S*,25(OH)$_2$D$_3$ in stimulating the expression of *CYP24A1* in comparison to other secosteroids could be secondary to its very efficient hydroxylation by CYP27B1 (Table 1) [66].

We also found that the newly-synthesized secosteroids interacted with the AhR (Fig. 5B, D, Table 2), similar to our previous study [62] except that 20*S*,23*R*(OH)$_2$D$_3$ was found to act as a reverse agonist. Molecular modeling predicts that 20*S*(OH)D$_3$, 20*S*,25(OH)$_2$D$_3$, 20*S*,23*S*(OH)$_2$D$_3$ and 20*S*,23*R*(OH)$_2$D$_3$ share the same binding region in AhR. 20*S*(OH)D$_3$ and 20*S*,25(OH)$_2$D$_3$ have the similar binding postures with AhR, while the binding postures of 20*S*,23*R*(OH)$_2$D$_3$ and 20*S*,23*S*(OH)$_2$D$_3$ with AhR are very similar (Fig. 6a).

The binding between AhR and D$_3$ derivatives is mainly through hydrophobic interactions. Hydrophobic residues Cys333, Phe295, Phe287, Tyr322, Leu308, Tyr310, Leu315, Leu353, Ile325, Val381 and Ala367 in AhR are directly involved in the binding with all four molecules of 20*S*(OH)D$_3$, 20*S*,25(OH)$_2$D$_3$, 20*S*,23*S*(OH)$_2$D$_3$ and 20*S*,23*R*(OH)$_2$D$_3$ (Fig. 6a (B)). Recently we have reported that 20*S*(OH)D$_3$, 20*S*,23(OH)$_2$D$_3$, 20*S*,25(OH)$_2$D$_3$ and other D$_3$-hydroxy derivatives can act as ligands on LXR [61]. Therefore, we compared interactions of 20*S*,23*S*(OH)$_2$D$_3$ versus 20*S*,23*R*(OH)$_2$D$_3$ with the LBD of LXRα and β (Fig. 5E, F) using a functional assay and molecular modeling (Table 2, Fig. 6b). The functional assays using LanthaScreen TR-FRET LXRα and β coactivator assays has confirmed that 20*S*,23(OH)$_2$D$_3$ isomers are agonists on the LXRα and β [61], with some differences (Fig. 5E, F). Vitamin D$_3$ derivatives had better affinity on LXRβ than on LXRα. When binding with LXRs, 20*S*(OH)D$_3$, 20*S*,25(OH)$_2$D$_3$, 20*S*,23*S*(OH)$_2$D$_3$ and 20*S*,23*R*(OH)$_2$D$_3$ all bind to the same binding pocket of either LXRα or LXRβ (Fig. 6b (A) and (B)). For LXRα, 20*S*(OH)D$_3$ and 20*S*,25(OH)$_2$D$_3$ have the similar binding postures, whereas 20*S*,23*S*(OH)$_2$D$_3$ and 20*S*,23*R*(OH)$_2$D$_3$ have the similar binding posture but twisted from C20 compared to that of 20*S*(OH)D$_3$ and 20*S*,25(OH)$_2$D$_3$ (Fig. 6b (A) and (C)). For LXRβ, similar observation based on 2D and 3D interaction maps(Fig. 6b (B) and (D)). 20*S*,23*S*(OH)$_2$D$_3$ has a better affinity with LXRβ compared to that of 20*S*,23*R*(OH)$_2$D$_3$ (Table 2), which is also observed in experimental data (Fig. 5E, F). 20*S*(OH)D$_3$, 20*S*,25(OH)$_2$D$_3$, 20*S*,23*S*(OH)$_2$D$_3$ and 20*S*,23*R*(OH)$_2$D$_3$ binding postures to LXRα (Fig. 6b (C)) are very similar to their binding postures to LXRβ (Fig. 6b (D)).

The binding between LXRα and D$_3$ derivatives is mainly through hydrophobic interactions. Hydrophobic residues Ile295, Phe335, Met298, Leu299, Phe315, Leu316, Ala261, Leu260, Phe257 and Le439 in LXRα are directly involved in the binding with all four molecules of 20*S*(OH)D$_3$, 20*S*,25(OH)$_2$D$_3$, 20*S*,23*S*(OH)$_2$D$_3$ and 20*S*,23*R*(OH)$_2$D$_3$ (Fig. 6b (C)). The binding of 20*S*(OH)D$_3$ to LXRα involved the formation of a hydrogen bond between the hydroxyl group on C3 of 20*S*(OH)D$_3$ with Leu316, while the binding of 20*S*,23*S*(OH)$_2$D$_3$ with LXRβ involved formation of a hydrogen bond between the 23-hydroxyl group of 20*S*,23*S*(OH)$_2$D$_3$ and Leu274 (Fig. 6b (D)).

Lastly, we performed molecular modeling of 20*S*(OH)D$_3$, 20*S*,25(OH)$_2$D$_3$, 20*S*,23*S*(OH)$_2$D$_3$ and 20*S*,23*R*(OH)$_2$D$_3$ with LBD of the RORs (Fig. 6c, Table 2). 20*S*(OH)D$_3$, 20*S*,25(OH)$_2$D$_3$, 20*S*,23*S*(OH)$_2$D$_3$ and 20*S*,23*R*(OH)$_2$D$_3$ all bind to the same binding pocket of both RORα and RORγ (Fig. 6c (A) and (B)). For RORα,

20*S*(OH)D_3 and 20*S*,25(OH)$_2D_3$ share a similar binding posture to each other, distinct from 20*S*,23*S*(OH)$_2D_3$ and 20*S*,23*R*(OH)$_2D_3$ which are also similar to each other (Fig. 6c (C)). For RORγ, again 20*S*(OH)D_3 and 20*S*,25(OH)$_2D_3$ show similar binding postures to each other, as do 20*S*,23*R*(OH)$_2D_3$ and 20*S*,23*S*(OH)$_2D_3$ (Fig. 6c (D)). The bindings between RORs and D_3 derivatives are mainly mediated through hydrophobic interactions. Hydrophobic residues Ile327, Tyr290, Met368, Val379, Tyr380, Val364, Val403, Phe391 and Ile400 in RORα are directly involved in the binding with all four D_3 derivatives (Fig. 6c (C)). Hydrophobic residues Leu287, Phe378, Phe377, Val376, Ile397, Ile400, Phe388, Leu391, Cys320 and Leu324 in RORγ are directly involved in the binding with all four molecules of 20*S*(OH)D_3, 20*S*,25(OH)$_2D_3$, 20*S*,23*S*(OH)$_2D_3$ and 20*S*,23*R*(OH)$_2D_3$ (Fig. 6c (D)). These modeling data not only support our previous studies identifying novel hydroxy derivatives of D_3 as inverse agonists on RORs [58, 60], but also extend such observations to include 20*S*,23*R*(OH)$_2D_3$ and 20*S*,25(OH)$_2D_3$.

In summary, chemically synthesized 20*S*(OH)D_3, 20*S*,23*S*(OH)$_2D_3$, 20*S*,23*R*(OH)$_2D_3$ and 20*S*,25(OH)$_2D_3$ showed the ability to act on the VDR, AhR, LXR and ROR, consistent with our previous reports [57–62, 75], with some differences as indicated above. These studies provide a background for future exciting studies on the exact nature of these interactions between the secosteroids and their receptors, and the differences between different analogs.

Different vitamin D compounds have distinct and overlapping effects on activation of T cells in human peripheral blood

To determine if different vitamin D_3 compounds variably alter activation human CD4 and CD8 T cell, PBMC from healthy individuals were stimulated with anti-CD3 and anti-CD28 to activate T cells in the absence (ethanol) or presence of 20*S*(OH)D_3, 20*S*,23*S*(OH)$_2D_3$, 20*S*,23*R*(OH)$_2D_3$, 20*S*,25(OH)$_2D_3$ or 1α,25(OH)$_2D_3$ for 24 h. The cells were stained for the expression of lineage markers (CD4, CD8, CD14, CD19) and activation induced markers (AIM; CD69, ICOS, OX40, CD137, PD1 and HLADR) [76, 77]. We analyzed the data using an unsupervised algorithm-based approach combining TriMAP followed by self-organizing map (FlowSOM) cluster overlay as described in the Experimental section (Fig. 7A and 7B). Unsupervised algorithm-based analyses of multi-dimensional data enables unbiased identification of discovery as well as changes in cell populations [78,79]. Based on the expression levels of CD4, CD8 and the AIM, we identified four populations each of CD4 and CD8 T cells. Populations 2 and 4 within CD4 T cells were differentially altered by the vitamin D_3 compounds (Fig. 7A). For example, compared to ethanol treated cells, 1α,25(OH)$_2D_3$, 20*S*,23*S*(OH)$_2D_3$ and 20*S*,25(OH)$_2D_3$ treated cells contained fewer cells that down modulated CD4 and expressed increased levels of CD69 and ICOS (population 4, Fig. 7B). In contrast, 20*S*(OH)D_3 treatment increased the proportion of cells with population 4 phenotype and 20*S*,23(OH)$_2D_3$ had no effect on this population. Within CD8 T cells population 6 (cells that express ICOS) were differentially modulated by the vitamin D_3 compounds compared to ethanol treated cells (Fig 7A and 7B). . The unbiased algorithm-based computational analysis which used statistical “R code” reveals with accuracy that the different vitamin D compounds have overlapping and distinct effects in their ability to modulate T cell activation.

Concluding remarks

Efficient chemical synthetic routes for 20*S*(OH)D_3, 20*S*,23*S*$(OH)_2D_3$, 20*S*,23*R*$(OH)_2D_3$, and 20*S*,25$(OH)_2D_3$ were established. Convergent synthesis was used for the preparation of these target compounds where the key stage was a Wittig-Horner coupling of the corresponding Grundmann ketone (CD-ring fragment) with A-ring phosphine oxide. The resulting secosteroids were substrates for 1α-hydroxylation by CYP27B1 with the following selectivity: 20*S*,25$(OH)_2D_3$ >> 20*S*,23*S*$(OH)_2D_3$ > 20*S*(OH)D_3 = 20*S*,23*R*$(OH)_2D_3$. Functional assays and molecular modeling have shown that they act on the VDR, AhR, LXR and RORα and γ with some notable differences. 20*S*,25$(OH)_2D_3$ showed stronger stimulation of *CYP24A1*, a gene downstream of the VDR, than the other secosteroids which may be explained by its more efficient hydroxylation by CYP27B1. On the other hand, there was an interesting change from agonistic activity of 20*S*,23*S*$(OH)_2D_3$ on the AhR to inverse agonism by its 23*R*-isomer (20*S*,23*R*$(OH)_2D_3$). In addition, 20*S*,23*R*$(OH)_2D_3$ was less efficient in activation of LXRβ than 20*S*,23*S*$(OH)_2D_3$. This work provides the background for future studies on the different modes of nuclear receptor signaling by hydroxy-D_3 derivatives under study. Interestingly, the major phenotypic effects caused by the synthesized secosteroids were very similar and included inhibition of cell proliferation in skin cells and induction of keratinocyte differentiation. Finally, these secosteroids showed immunomodulatory effects on human PBMC stimulated by coactivating peptides with net effects of downregulation of proinflammatory responses. Interestingly, the pattern of expression of lymphocytic markers was both overlapping and differential indicating a difference in mechanism of action depending on the position of the OH group and its configuration in the D_3 side chain. These secosteroids showed differential effects in comparison to classical 1α,25$(OH)_2D_3$. This work underpins new possibilities for exciting studies on the anti-inflammatory actions of the D_3 hydroxy derivatives in order to establish efficient methods to treat inflammatory and autoimmune diseases.

In summary, new efficient routes of chemical synthesis for 20*S*(OH)D_3, 20*S*,23*S*$(OH)_2D_3$, 20*S*,23*R*$(OH)_2D_3$, and 20*S*,25$(OH)_2D_3$ were designed allowing their production for in vivo testing and further clarification of different mechanisms of action as well as future preclinical studies on autoimmune disorders including lupus erythematosus, rheumatoid arthritis, inflammatory bowel disease, psoriasis and multiple sclerosis.

Experimental Section

Chemistry

Optical rotations were measured in chloroform using a Perkin-Elmer model 343 polarimeter (Shelton, CT, USA). Ultraviolet (UV) absorption spectra were obtained on a Shimadzu UV-1800 spectrophotometer (Kyoto, Japan) in absolute ethanol. Nuclear magnetic resonance spectra were recorded in $CDCl_3$ solutions using Bruker AVANCE 300 MHz (Karlsruhe, Germany) and Bruker AVANCE 500 MHz instruments. Chemical shifts (δ) are reported in parts per million relative to $(CH_3)_4Si$ (δ 0.00) or the solvent signal as an internal standard. Abbreviations used are singlet (s), doublet (d), triplet (t), quartet (q), multiplet (m), broad (br), narrow (narr). High-resolution mass spectra were recorded on Shimadzu LCMS-IT-TOF mass spectrometer using electrospray ionization (ESI) technique.

Reactions were carried out with magnetic stirring. All reactions involving moisture- or oxygen-sensitive compounds were carried out under dry argon atmosphere. Reaction temperatures refer to external bath temperatures. Tetrahydrofuran was distilled from Na/benzophenone; dichloromethane was distilled from P_2O_5. The organic extracts were dried over anhydrous $MgSO_4$, filtered and concentrated using a rotary evaporator with vacuum pump attached. Reactions were monitored by thin-layer chromatography (TLC) using aluminum-backed MERCK 60 silica gel plates (Darmstadt, Germany) (0.2 mm thickness). The chromatograms were visualized first with ultraviolet light (254 nm) and then by immersion in a cerium-molybdenum solution [10 g $Ce(SO_4)_2 \times 4\ H_2O$, 25 g phosphomolybdic acid, 60 mL H_2SO_4 and 940 mL H_2O] or *p*-anisaldehyde solution (5 mL H_2SO_4, 1.5 mL glacial AcOH, 3.7 mL *p*-anisaldehyde, 135 mL H_2O) followed by heating.

The purity of final compounds was determined by HPLC and they were judged at least 98% pure. For this purpose, straight-phase (SP) and reversed-phase (RP) high-performance liquid chromatography were performed on Shimadzu Prominence system equipped with SPD 20A UV detector (265 nm). For straight-phase a Zorbax RX-SIL semi-preparative 9.4 × 250 mm, 5 μm column and for reverse-phase a Zorbax Eclipse XDB-C18 semi-preparative 9.4 × 250 mm, 5 μm HPLC column were used. The purity and identity of the synthesized secosteroids were additionally confirmed by inspection of their ^{1}H NMR, ^{13}C NMR and high-resolution mass spectra (HRMS).

(1*S*,3a*R*,4*S*,7a*S*)-1-[(*S*)-2'-Hydroxy-6'-methylheptan-2'-yl]-7a-methyloctahydro-1H-inden-4-ol (13).—To a suspension of activated magnesium turnings (105 mg, 4.40 mmol) in anhydrous THF (7 mL) was added a small crystal of iodine and 1-bromo-4-methylpentane (0.22 mL, 1.48 mmol). The mixture was heated to the boiling point and second portion of 1-bromo-4-methyl-pentane (0.22 mL, 1.48 mmol) was added. Stirring was continued for 1 h and then the mixture was cooled to 0 °C. The generated Grignard reagent was then added to a solution of ketone **12** (70 mg, 0.295 mmol) in anhydrous THF (3 mL) at 0 °C and the stirring was continued for 2 h at this temperature and overnight at room temperature. The mixture was diluted with diethyl ether (10 mL) and saturated solution of NH_4Cl (10 mL) was carefully added at 0 °C. The layers were separated and the aqueous was extracted with AcOEt (2 × 10 mL). The combined organic solvents were dried ($MgSO_4$) and concentrated. The residue was purified by column chromatography on silica using hexane/ethyl acetate (84:16) to give the compound **13** (70 mg, 85%) as a colorless oil. **13**: $[\alpha]_D^{24}$+21 (*c* 0.6, $CHCl_3$); ^{1}H NMR (300 MHz, $CDCl_3$) δ 0.88 (6H, d, *J* = 6.6 Hz, 6'-CH_3 and 7'-H_3), 1.15 (3H, s, 7a-CH_3), 1.27 (3H, s, 1'-H_3), 4.10 (1H, narr m, 4α-H); ^{13}C NMR (75 MHz) δ 15.4, 17.4, 21.3, 21.9, 22.2, 22.5, 22.7, 26.3, 27.9, 33.4, 39.6, 40.8, 42.5, 44.1, 52.6, 57.9, 69.4, 75.1; HRMS (ESI) calcd. for $C_{18}H_{34}O_2Na$ (M^++ Na) 305.2457, measured 305.2462.

(1*S*,3a*R*,4*S*,7a*S*)-1-[(*S*)-2'-Hydroxy-6'-methyl-6'-[(triethylsilyl)oxy]heptan-2'-yl]-7a-methyloctahydro-1H-inden-4-ol (14).—The reaction of the ketone **12** (90 mg, 0.377 mmol) with the Grignard reagent, generated from 1-bromo-4-methyl-4-[(triethylsilyl)oxy]pentane, was performed as described above for **13**. After the analogous procedure, the crude product was purified by column chromatography on silica

using hexane/ethyl acetate (86:14) to give **14** (124 mg, 85%) as a colorless oil. **14**: $[\alpha]_D^{24}$+16 (*c* 0.95, $CHCl_3$); ^{1}H NMR (300 MHz, $CDCl_3$) δ 0.56 (6H, q, *J* = 7.5 Hz, 3 × $SiC\underline{H}_2CH_3$), 0.94 (9H, t, *J* = 7.5 Hz, 3 × $SiCH_2C\underline{H}_3$), 1.14 (3H, s, 7a-CH_3), 1.19 (6H, s, 6'-CH_3 and 7'-H_3), 1.27 (3H, s, 1'-H_3), 4.09 (1H, narr m, 4α-H); ^{13}C NMR (75 MHz) δ 6.8, 7.1, 15.4, 17.4, 19.0, 21.4, 22.2, 26.3, 29.8, 30.1, 33.4, 40.8, 42.6, 44.4, 45.6, 52.6, 57.9, 69.5, 73.4, 75.2; HRMS (ESI) calcd. for $C_{24}H_{48}O_3SiNa$ (M^++ Na) 435.3270, measured 435.3279.

(1*S*,3a*R*,7a*R*)-1-[(*S*)-2'-Hydroxy-6'-methylheptan-2'-yl]-7a-methyloctahydro-4H-inden-4-one (15).—Molecular sieves 4 Å (70 mg) were added to a solution of the diol **13** (70 mg, 0.247 mmol) in anhydrous CH_2Cl_2 (2 mL) and the mixture was cooled to 0 °C. 4-Methylmorpholine *N*-oxide (NMO, 44 mg, 0.371 mmol) and tetrapropylammonium perruthenate (TPAP, 44 mg, 0.124 mmol) were then added. The resulted dark mixture was stirred for 1.5 h and then filtered through Celite. The solvent was evaporated and the residue was purified by column chromatography on silica using hexane/ethyl acetate (86:14) to give the ketone **15** (53 mg, 77%) as a colorless oil. **15**: $[\alpha]_D^{24}$−21 (*c* 1.5, $CHCl_3$); ^{1}H NMR (300 MHz, $CDCl_3$) δ 0.83 (3H, s, 7a-CH_3), 0.89 (6H, d, *J* = 6.6 Hz, 6'-CH_3 and 7'-H_3), 1.31 (3H, s, 1'-H_3), 2.45 (1H, dd, *J* = 10.7, 7.0 Hz, 3a-H); ^{13}C NMR (75 MHz) δ 14.4, 18.8, 21.8, 22.0, 22.6, 22.7, 23.9, 25.6, 27.9, 39.3, 39.5, 40.8, 44.1, 49.8, 58.2, 62.2, 74.6, 211.9; HRMS (ESI) calcd. for $C_{18}H_{32}O_2Na$ (M^++ Na) 303.2300, measured 303.2295.

(1*S*,3a*R*,7a*R*)-1-[(*S*)-2'-Hydroxy-6'-methyl-6'-[(triethylsilyl)oxy]heptan-2'-yl]-7a-methyloctahydro-4H-inden-4-one (16).—The oxidation of the secondary hydroxyl group in **14** (145 mg, 0.353 mmol) was performed analogously as described above for **13**. The crude product was purified by column chromatography over silica using hexane/ethyl acetate (88:12) to give the ketone **16** (115 mg, 80%) as a colorless oil. **16**: $[\alpha]_D^{24}$−13 (c 1.0, $CHCl_3$); ^{1}H NMR (300 MHz, $CDCl_3$) δ 0.56 (6H, q, *J* = 7.5 Hz, 3 × $SiC\underline{H}_2CH_3$), 0.81 (3H, s, 7a-CH_3), 0.94 (9H, t, *J* = 7.5 Hz, 3 × $SiCH_2C\underline{H}_3$), 1.20 (6H, s, 6'-CH_3 and 7'-H_3), 1.30 (3H, s, 1'-H_3), 2.42 (1H, dd, *J* = 10.5, 6.9 Hz, 3a-H); ^{13}C NMR (75 MHz) δ 6.8, 7.1, 14.4, 18.8, 19.0, 21.8, 24.0, 26.6, 29.8, 30.1, 39.3, 40.8, 44.4, 45.5, 49.8, 58.1, 62.2, 73.3, 74.7, 211.9; HRMS (ESI) calcd. for $C_{24}H_{46}O_3SiNa$ (M^++ Na) 433.3114, measured 433.3122.

(1*S*,3a*R*,7a*R*)-7a-Methyl-1-[(*S*)-6'-methyl-2'-[(trimethylsilyl)oxy]heptan-2'-yl]octahydro-4H-inden-4-one (17).—To a solution of hydroxy ketone **15** (76 mg, 0.271 mmol) in anhydrous CH_2Cl_2 (2 mL) was added 2,6-lutidine (63 μL, 0.542 mmol) and trimethylsilyl trifluoromethanesulfonate (74 μL, 0.406 mmol) at −78 °C and the mixture was stirred at this temperature for 1 h. Saturated $NaHCO_3$ (2 mL) was added and the mixture was extracted with dichloromethane (3 × 5 mL). The combined organic layers were washed with 5% HCl (5 mL), water (5 mL), dried ($MgSO_4$) and evaporated. The residue was purified by column chromatography on silica using hexane/ethyl acetate (99:1) to give protected ketone **17** (80 mg, 84%) as a colorless oil. **17**: $[\alpha]_D^{24}$−12 (*c* 1.4, $CHCl_3$); ^{1}H NMR (300 MHz, $CDCl_3$) δ 0.076 [9H, s, $Si(CH_3)_3$], 0.75 (3H, s, 7a-CH_3), 0.87 (6H, d, *J* = 6.6 Hz, 6'-CH_3 and 7'-H_3), 1.32 (3H, s, 1'-H_3), 2.39 (1H, dd, *J* = 10.8, 6.9 Hz, 3a-H); ^{13}C NMR (75 MHz) δ 2.8, 14.4,

18.8, 21.8, 22.6, 22.7, 23.2, 24.0, 27.8, 27.9, 39.6, 39.8, 40.9, 45.0, 49.9, 57.4, 62.3, 78.0, 212.3; HRMS (ESI) calcd. for $C_{21}H_{40}O_2SiNa$ (M^++ Na) 375.2695, measured 375.2702.

(1*S*,3a*R*,7a*R*)-7a-Methyl-1-[(*S*)-6'-methyl-6'-[(triethylsilyl)oxy]-2'-[(trimethylsilyl)oxy]heptan-2'-yl]octahydro-4H-inden-4-one (18).—Protection of tertiary hydroxyl group in **16** (115 mg, 0.281 mmol) was performed analogously as described above for **15**. The crude product was purified by column chromatography over silica using hexane/ethyl acetate (99:1) to give protected ketone **18** (111 mg, 82%) as a colorless oil. **18**: $[\alpha]_D^{24}$−9 (*c* 1.0, $CHCl_3$); ^{1}H NMR (300 MHz, $CDCl_3$) δ 0.078 [9H, s, $Si(CH_3)_3$], 0.57 (6H, q, *J* = 7.5 Hz, 3 × $SiC\underline{H}_2CH_3$), 0.75 (3H, s, 7a-CH_3), 0.95 (9H, t, *J* = 7.5 Hz, 3 × $SiCH_2C\underline{H}_3$), 1.20 (6H, s, 6'-CH_3 and 7'-H_3), 1.32 (3H, s, 1'-H_3), 2.38 (1H, dd, *J* = 10.8, 6.8 Hz, 3a-H); ^{13}C NMR (75 MHz) δ 2.8, 6.8, 7.1, 14.4, 18.8, 20.1, 21.9, 24.0, 27.8, 29.9, 30.1, 39.6, 40.9, 45.2, 45.8, 49.9, 57.5, 62.4, 73.2, 78.1, 212.4; HRMS (ESI) calcd. for $C_{27}H_{54}O_3Si_2Na$ (M^++ Na) 505.3509, measured 505.3515.

(20*S*)-3-[(*tert*-Butyldimethylsilyl)oxy]-20-[(trimethylsilyl)oxy]vitamin D_3 (19).— To a solution of phosphine oxide **9** (395 mg, 0.860 mmol) in anhydrous THF (5 mL) was added *n*-BuLi (540 μL, 0.870 mmol) at −78 °C and the stirring of a deep red solution was continued for 30 min. A solution of the ketone **17** (154 mg, 0.430 mmol) in anhydrous THF (2 mL) was then added and the stirring was continued for 3 h. Saturated NH_4Cl (3 mL) was added and the mixture was extracted with diethyl ether (3 × 5 mL). The combined organic layers were washed with water (5 mL), dried ($MgSO_4$) and evaporated. The crude product was purified by column chromatography using hexane to give protected vitamin D compound **19** (204 mg, 81%) as a colorless oil. **19**: $[\alpha]_D^{24}$+61 (*c* 1.5, $CHCl_3$); ^{1}H NMR (300 MHz, $CDCl_3$) δ 0.070 [9H, s, $Si(CH_3)_3$], 0.67 (3H, s, 18-H_3), 0.88 (6H, d, *J* = 6.6 Hz, 26- and 27-H_3), 0.90 (9H, s, Si-*t*-Bu), 1.29 (3H, s, 21-H_3), 2.12 (1H, m, 1α-H), 2.26 (1H, dd, *J* = 13.2, 9.6 Hz, 4β-H), 2.36 (1H, dt, *J* = 13.5, 4.6 Hz, 1β-H), 2.46 (1H, dd, *J* = 13.2, 4.5 Hz, 4α-H), 2.82 (1H, br d, *J* ~ 13 Hz, 9β-H), 3.82 (1H, tt, *J* = 9.6, 4.5 Hz, 3α-H), 4.80 and 5.01 (1H and 1H, each s, 19-H_2), 6.01 and 6.17 (1H and 1H, each d, *J* = 11.2 Hz, 7- and 6-H); ^{13}C NMR (75 MHz) δ −4.6, −4.5, 2.8, 13.9, 18.2, 21.9, 22.0, 22.6, 22.8, 23.3, 23.4, 25.9, 27.7, 27.9, 28.8, 32.8, 36.5, 39.8, 41.2, 45.2, 45.9, 46.9, 56.8, 57.5, 70.7, 78.5, 112.2, 118.1, 121.4, 136.2, 141.5, 145.4; HRMS (ESI) calcd. for $C_{36}H_{66}O_2Si_2Na$ (M^++ Na) 609.4499, measured 609.4508.

(20*S*)-3-[(*tert*-Butyldimethylsilyl)oxy]-25-[(triethylsilyl)oxy]-20-[(trimethylsilil)oxy]-vitamin D_3 (20).—The Wittig-Horner reaction between ketone **18** (44 mg, 0.092 mmol) and phosphine oxide **9** (83 mg, 0.184 mmol) was performed analogously as described above for **17**. The crude product was purified by column chromatography over silica using hexane/ethyl acetate (99:1) to give protected vitamin D compound **20** (60 mg, 91%) as a colorless oil. **20**: $[\alpha]_D^{24}$+54 (*c* 1.0, $CHCl_3$); ^{1}H NMR (300 MHz, $CDCl_3$) δ 0.069 [9H, s, $Si(CH_3)_3$], 0.57 (6H, q, *J* = 7.5 Hz, 3 × $SiC\underline{H}_2CH_3$), 0.66 (3H, s, 18-H_3), 0.90 (9H, s, Si-*t*-Bu), 0.95 (9H, t, *J* = 7.5 Hz, 3 × $SiCH_2C\underline{H}_3$), 1.20 (6H, s, 26- and 27-H_3), 1.30 (3H, s, 21-H_3), 2.12 (1H, m, 1α-H), 2.23 (1H, dd, *J* = 13.2, 9.3 Hz, 4β-H), 2.36 (1H, dt, *J* = 13.7, 4.8 Hz, 1β-H), 2.46 (1H, dd, *J* = 13.2, 4.2 Hz, 4α-H), 2.82 (1H, br d, *J* ~ 12

Hz, 9β-H), 3.81 (1H, tt, *J* = 9.3, 4.2 Hz, 3α-H), 4.80 and 5.00 (1H and 1H, each s, 19-H_2), 6.01 and 6.17 (1H and 1H, each d, *J* = 11.2 Hz, 7- and 6-H); ^{13}C NMR (75 MHz) δ −4.6, −4.5, 2.8, 6.8, 7.2, 13.9, 18.2, 20.2, 21.9, 22.0, 23.4, 25.9, 26.9, 27.7, 28.9, 29.8, 30.1, 32.8, 36.4, 41.1, 45.3, 45.8, 46.9, 56.8, 57.5, 70.7, 73.3, 78.6, 112.1, 118.1, 121.4, 136.2, 141.6, 145.4; HRMS (ESI) calcd. for $C_{42}H_{80}O_3Si_3Na$ (M^++ Na) 739.5313, measured 739.5322.

(20*S*)-20-Hydroxyvitamin D_3 (3).—Tetra-*n*-butylammonium fluoride (1M in THF; 4.3 mL, 4.3 mmol) was added to a solution of protected vitamin D compound **23** (84 mg, 0.143 mmol) in anhydrous THF (5 mL) and the mixture was stirred at room temperature overnight. Brine (3 mL) was added and the mixture was extracted with AcOEt (3 × 10 mL). The combined organic layers were washed with water (5 mL), dried ($MgSO_4$) and evaporated. The crude product was purified by HPLC (9.4 mm × 25 cm Zorbax-Sil column, 4 mL/min) using hexane/2-propanol (95:5) solvent system; vitamin **3** (48 mg, 84%) was collected at R_V = 23 mL. Analytical sample of the vitamin was obtained after reversed-phase HPLC (9.4 mm × 25 cm Zorbax Eclipse XDB-C18 column, 4 mL/min) using methanol/water (9:1) solvent system (R_V = 44 mL). **3**: $[\alpha]_D^{24}$+21 (*c* 1.1, $CHCl_3$); ^{1}H NMR (300 MHz, $CDCl_3$) δ 0.72 (3H, s, 18-H_3), 0.87 (6H, d, *J* = 6.6 Hz, 26- and 27-H_3), 1.27 (3H, s, 21-H_3), 2.17 (1H, ddd, *J* = 13.5, 8.5, 4.8 Hz, 1α-H), 2.28 (1H, dd, *J* = 13.2, 7.2 Hz, 4β-H), 2.39 (1H, ddd, *J* = 13.5, 7.6, 4.8 Hz, 1β-H), 2.57 (1H, dd, *J* = 13.2, 3.6 Hz, 4α-H), 2.82 (1H, br d, *J* ~ 13 Hz, 9β-H), 3.94 (1H, tt, *J* = 7.3, 3.6 Hz, 3α-H), 4.82 and 5.04 (1H and 1H, each s, 19-H_2), 6.03 and 6.23 (1H and 1H, each d, *J* = 11.2 Hz, 7- and 6-H); ^{13}C NMR (75 MHz) δ 13.7, 21.9, 22.0, 22.1, 22.6, 22.7, 23.4, 26.6, 27.9, 28.9, 31.9, 35.2, 39.6, 40.8, 43.9, 45.9, 46.0, 56.5, 58.2, 69.2, 75.2, 112.5, 118.2, 122.3, 135.4, 141.5, 145.0; HRMS (ESI) calcd. for $C_{27}H_{45}O_2$ (M^++ Na) 401.3420, measured 401.3428.

(20*S*)-20,25-Dihydroxyvitamin D_3 (6).—The hydroxyl deprotection in the vitamin D compound **24** (60 mg, 0.083 mmol) was performed analogously as described above for **23**. The crude product was purified by HPLC (9.4 mm × 25 cm Zorbax-Sil column, 4 mL/min) using hexane/2-propanol (9:1) solvent system; vitamin **6** (26 mg, 75%) was collected at R_V = 29 mL. Analytical sample of the vitamin was obtained after reversed-phase HPLC (9.4 mm × 25 cm Zorbax Eclipse XDB-C18 column, 4 mL/min) using methanol/water (8:2) solvent system (R_V = 37 mL). **6**: $[\alpha]_D^{24}$+20 (*c* 1.3, $CHCl_3$); ^{1}H NMR (300 MHz, $CDCl_3$) δ 0.72 (3H, s, 18-H_3), 1.22 (6H, s, 26- and 27-H_3), 1.28 (3H, s, 21-H_3), 2.17 (1H, ddd, *J* = 13.4, 8.5, 4.6 Hz, 1α-H), 2.28 (1H, dd, *J* = 13.2, 7.3 Hz, 4β-H), 2.40 (1H, ddd, *J* = 13.4, 7.5, 4.6 Hz, 1β-H), 2.57 (1H, dd, *J* = 13.2, 3.5 Hz, 4α-H), 2.81 (1H, br d, *J* ~ 13 Hz, 9β-H), 3.94 (1H, tt, *J* = 7.3, 3.5 Hz, 3α-H), 4.81 and 5.05 (1H and 1H, each s, 19-H_2), 6.03 and 6.22 (1H and 1H, each d, *J* = 11.2 Hz, 7- and 6-H); ^{13}C NMR (75 MHz) δ 13.8, 18.9, 21.9, 22.0, 23.3, 26.5, 28.8, 29.2, 29.5, 31.9, 35.2, 40.8, 43.9, 44.4, 45.8, 46.0, 56.5, 58.3, 69.2, 71.0, 75.2, 112.5, 118.2, 122.3, 135.5, 141.4, 145.1; HRMS (ESI) calcd. for $C_{27}H_{45}O_3$ (M^++ H) 417.3369, measured 417.3372.

(3*S*)-3-[(1'*S*,3a'*R*,4'*S*,7a'*S*)-7a'-Methyl-4'-[(triethylsilyl)oxy]-octahydro-1H-inden-1'-yl)]-3-hydroxybutanenitrile (21).—To a solution of acetonitrile (0.45 mL, 8.69 mmol) in anhydrous THF (20 mL) was added LDA (2M in THF/heptane/ethylbenzene; 4.3 mL, 8.60 mmol) at −78 °C. The yellow

mixture was stirred at this temperature for 30 min. A solution of ketone **11** (0.60 g, 1.93 mmol) in anhydrous THF (10mL) was added and stirring was continued for 2 h. Saturated NH_4Cl (10 mL) was slowly added and the mixture was extracted with ethyl acetate (3 × 15 mL). The combined organic layers were washed with water (10 mL), dried ($MgSO_4$) and evaporated. The residue was purified by column chromatography on silica using hexane/ethyl acetate (85:15) to give hydroxy nitrile **21** (0.624 g, 92%) as a colorless oil. **21**: $[\alpha]_D^{24}$ +29 (*c* 1.0, $CHCl_3$); ^{1}H NMR (300 MHz, $CDCl_3$) δ 0.54 (6H, q, *J* = 7.8 Hz, $SiC\underline{H}_2CH_3$), 0.94 (9H, t, *J* = 7.8 Hz, $SiCH_2C\underline{H}_3$), 1.11 (3H, s, 7a'-CH_3), 1.49 (3H, s, 4-H_3), 2.43 and 2.49 (1H and 1H, each d, *J* = 16.5 Hz, 2-H_2), 4.05 (1H, narr m, 4'α-H); ^{13}C NMR (75 MHz) δ 4.8, 6.9, 15.4, 17.5, 21.6, 22.6, 27.1, 32.4, 34.3, 40.8, 42.9, 52.9, 57.8, 69.2, 73.6, 117.9; HRMS (ESI) calcd. for $C_{20}H_{37}NO_2SiNa$ (M^++ Na) 374.2491, measured 374.2495.

(3*S*)-3-[(1'*S*,3a'*R*,4'*S*,7a'*S*)-4'-Hydroxy-7a'-methyl-octahydro-1H-inden-1'-yl)]-3-hydroxybutanenitrile (22).—To a solution of nitrile **21** (0.458 g, 1.30 mmol) in CH_2Cl_2 (20 mL) was added a solution of hydrogen chloride in dioxane (4 M; 0.98 mL, 3.92 mmol) at 0 °C and the mixture was stirred for 30 min. Then, water (5 mL) and $NaHCO_3$ (10 mL) were added and the layers were separated. The aqueous phase was extracted with dichloromethane (2 × 10 mL) and the combined organic layers were washed with water (10 mL), dried ($MgSO_4$) and evaporated. The residue was purified by column chromatography on silica using hexane/ethyl acetate (7:3) to give diol **22** (0.302 g, 98%) as a colorless oil. **22**: $[\alpha]_D^{24}$+14 (*c* 1.0, $CHCl_3$); ^{1}H NMR (300 MHz, $CDCl_3$) δ 1.13 (3H, s, 7a'-CH_3), 1.51 (3H, s, 4-H_3), 2.44 and 2.50 (1H and 1H, each d, *J* = 16.6 Hz, 2-H_2), 4.10 (1H, narr m, 4'-H); ^{13}C NMR (75 MHz) δ 15.3, 17.3, 21.5, 22.1, 27.1, 32.6, 33.4, 40.5, 42.8, 52.4, 57.6, 69.1, 73.5, 117.8; HRMS (ESI) calcd. for $C_{14}H_{23}NO_2Na$ (M^++ Na) 260.1626, measured 260.1620.

(3*S*)-3-Hydroxy-3-[(1'*S*,3a'*R*,7a'*R*)-7a'-methyl-4'-oxo-octahydro-1H-inden-1'-yl)butanenitrile (23).—The oxidation of the secondary hydroxyl group in **22** (73 mg, 0.307 mmol) was performed analogously as described above for **13**. The crude product was purified by column chromatography over silica using hexane/ethyl acetate (7:3) to give the ketone **23** (68 mg, 95%) as a colorless oil. **23**: $[\alpha]_D^{24}$−19 (*c* 0.97, $CHCl_3$); ^{1}H NMR (300 MHz, $CDCl_3$) δ 0.80 (3H, s, 7a'-CH_3), 1.55 (3H, s, 4-H_3), 2.48 and 2.55 (1H and 1H, each d, *J* = 16.5 Hz, 2-H_2); ^{13}C NMR (75 MHz) δ 14.2, 18.8, 21.9, 23.7, 27.5, 32.5, 38.9, 40.7, 49.7, 57.7, 61.8, 73.0, 117.6, 211.1; HRMS (ESI) calcd. for $C_{14}H_{21}NO_2Na$ (M^++ Na) 258.1470, measured 258.1465.

(3*S*)-3-[(1'*S*,3a'*R*,7a'*R*)-7a'-methyl-4'-oxo-octahydro-1H-inden-1'-yl)]-3-[(trimethylsilyl)oxy]butanenitrile (24).—To a solution of hydroxy nitrile **23** (89 mg, 0.378 mmol) in anhydrous CH_2Cl_2 (4 mL) was added pyridine (300 μL, 3.78 mmol) and trimethylsilyl trifluoromethanesulfonate (206 μL, 1.14 mmol) at 0 °C and the mixture was stirred at this temperature for 1 h. Saturated $NaHCO_3$ (3 mL) was added and the mixture was extracted with dichloromethane (3 × 5 mL). The combined organic layers were washed with 5% HCl (5 mL), water (5 mL), dried ($MgSO_4$) and evaporated. The residue was purified by column chromatography on silica using hexane/ethyl acetate (9:1) to give ketone **24** (101 mg, 86%) as a colorless oil. **24**: $[\alpha]_D^{24}$−15

(*c* 0.97, $CHCl_3$); ^{1}H NMR (300 MHz, $CDCl_3$) δ 0.14 [9H, s, $Si(CH_3)_3$], 0.75 (3H, s, 7a'-CH_3), 1.57 (3H, s, 4-H_3), 2.41 and 2.49 (1H and 1H, each d, *J* = 16.4 Hz, 2-H_2); ^{13}C NMR (75 MHz) δ 2.4, 14.2, 18.8, 22.0, 23.8, 27.9, 32.5, 39.2, 40.7, 49.7, 58.5, 61.9, 75.9, 117.8, 211.4; HRMS (ESI) calcd. for $C_{17}H_{29}NO_2SiNa$ (M^++ Na) 330.1865, measured 330.1870.

(20*S*)-3-[(*tert*-Butyldimethylsilyl)oxy]-22-cyano-20-[(trimethylsilyl)oxy]-23,24,25,26,27-pentanorvitamin D_3 (25).—The Wittig-Horner reaction between ketone **24** (100 mg, 0.325 mmol) and phosphine oxide **11** (294 mg, 0.650 mmol) was performed analogously as described above for **17**. The crude product was purified by column chromatography over silica using hexane/ethyl acetate (96:4) to give protected vitamin D compound **25** (152 mg, 87%) as a colorless oil. **25**: $[\alpha]_D^{24}$+52.6 (*c* 1.0, $CHCl_3$); ^{1}H NMR (300 MHz, $CDCl_3$) δ 0.064 and 0.070 (3H and 3H, each s, 2 × $SiCH_3$), 0.14 [9H, s, $Si(CH_3)_3$], 0.66 (3H, s, 18-H_3), 0.88 (9H, s, Si-*t*-Bu), 1.54 (3H, s, 21-H_3), 2.23 (1H, dd, *J* = 13.0, 9.1 Hz, 4β-H), 2.36 (1H, m, 1β-H), 2.40 and 2.55 (1H and 1H, each d, *J* = 16.3 Hz, 22-H_2), 2.44 (1H, dd, *J* = 13.0, 3.1 Hz, 4α-H), 2.82 (1H, br d, *J* ~ 12 Hz, 9β-H), 3.82 (1H, tt, *J* = 9.1, 4.3 Hz, 3α-H), 4.78 and 5.01 (1H and 1H, each s, 19-H_2), 6.01 and 6.15 (1H, and 1H, each d, *J* = 11.2 Hz, 6- and 7-H); ^{13}C NMR (75 MHz) δ −4.6, −4.5, 2.5, 13.7, 18.2, 21.9, 22.3, 23.2, 25.9, 27.8, 28.7, 32.5, 32.8, 36.4, 40.8, 45.9, 46.9, 56.4, 58.9, 70.6, 76.5, 112.2, 118.2, 118.6, 121.2, 136.8, 140.5, 145.5; HRMS (ESI) calcd. for $C_{32}H_{55}NO_2Si_2Na$ (M^++ Na) 564.3669, measured 564.3675.

(20*S*)-3-[(*tert*-Butyldimethylsilyl)oxy]-22-formyl-20-[(trimethylsilyl)oxy]-23,24,25,26,27-pentanorvitamin D_3 (26).—To a solution of nitrile **25** (105 mg, 0.193 mmol) in anhydrous CH_2Cl_2 (5 mL) was added diisobutylaluminum hydride (1.20 mL, 1.20 mmol) at −10 °C. Potassium sodium tartrate solution (2 mL) was added after 1 h and the mixture was extracted with CH_2Cl_2 (3 × 5 mL). The combined organic layers were washed with water, dried ($MgSO_4$) and evaporated. The crude product was purified by column chromatography using hexane/ethyl acetate (98:2) to give aldehyde **26** (65 mg, 62%) as a colorless oil. **26**: $[\alpha]_D^{24}$+50.5 (*c* 1.4, $CHCl_3$); ^{1}H NMR (300 MHz, $CDCl_3$) δ 0.08 and 0.09 (3H and 3H, each s, 2 × $SiCH_3$), 0.14 [9H, s, $Si(CH_3)_3$], 0.70 (3H, s, 18-H_3), 0.91 (9H, s, Si-*t*-Bu), 1.53 (3H, s, 21-H_3), 2.25 (1H, m, 4β-H), 2.39 (1H, dt, *J* =13.6, 4.8 Hz, 1β-H), 2.42 (1H, dd, *J* = 13.2, 4.5 Hz, 4α-H), 2.50 and 2.65 (1H and 1H, each dd, *J* = 14.0, 3.4 Hz, 22-H_2), 2.83 (1H, br d, *J* ~ 11.5 Hz, 9β-H), 3.84 (1H, tt, *J* = 9.0, 4.0 Hz, 3α-H), 4.80 and 5.03 (1H and 1H, each m, 19-H_2), 6.03 and 6.17 (1H and 1H, each d, *J* = 11.2 Hz, 7- and 6-H), 9.79 (1H, t, *J* = 3.4 Hz, CHO; ^{13}C NMR (75 MHz) δ −4.61, −4.60, 2.6, 14.0, 18.2, 21.9, 22.6, 23.3, 25.9, 28.7, 28.8, 32.8, 36.4, 41.0, 46.1, 46.9, 56.5, 57.5, 60.4, 70.6, 76.9, 112.2, 118.5, 121.2, 136.6, 140.7, 145.4, 202.1; HRMS (ESI) calcd. for $C_{32}H_{56}O_3Si_2Na$ (M^++ Na) 567.3666, measured 567.3678.

(20*S*,23*R*)- and (20*S*,23*S*)-3-[(*tert*-Butyldimethylsilyl)oxy]-23-hydroxy-20-[(trimethylsilyl)oxy]-vitamin D_3 (27a,b).—To a solution of aldehyde **26** (37 mg, 0.068 mmol) in anhydrous THF (2 mL) was added isobutylmagnesium chloride (2 M in THF; 68 μL, 0.136 mmol) at 0 °C and the mixture was stirred at rt overnight. Then, saturated NH_4Cl (1 mL) was added and the mixture was extracted with AcOEt (3 × 3 mL). The combined organic layers were washed with water (2 mL), dried ($MgSO_4$) and evaporated. The crude

product was purified by column chromatography using hexane/ethyl acetate (95:5) to give mixture of alcohols **27a,b** (29 mg, 70%) as a colorless oil.

(20*S*,23*R*)- and (20*S*,23*S*)-20,23-Dihydroxyvitamin D_3 (4a,b).—The hydroxyl deprotection in the vitamin D compounds **31a**,**b** (54 mg, 0.090 mmol) was performed analogously as described above for **23**. The products were separated by RP-HPLC (9.4 mm × 25 cm Zorbax Eclipse XDB-C18 column, 4 mL/min) using methanol/water (85:15) solvent system. Pure vitamin **4b** (16 mg) was collected at R_V = 28 mL and **4a** (11 mg) at Rv = 48 mL (total yield 74%).

4a: $[\alpha]_D^{24}$+25.1 (c 0.9, $CHCl_3$); ^{1}H NMR (300 MHz, $CDCl_3$) δ 0.63 (3H, s, 18-H_3), 0.92 (6H, d, *J* = 6.6 Hz, 26- and 27-H_3), 1.30 (3H, s, 21-H_3), 2.17 (1H, ddd, *J* = 13.1, 8.6, 4.7 Hz, 1α-H), 2.27 (1H, dd, *J* = 13.1, 7.6 Hz, 4β-H), 2.39 (1H, m, 1β-H), 2.56 (1H, dd, *J* = 13.1, 3.8 Hz, 4α-H), 2.82 (1H, dd, *J* = 11.8, 3.9 Hz, 9β-H), 3.93 (1H, m, 3α-H), 4.13 (1H, m, 23-H), 4.80 and 5.04 (1H and 1H, each m, 19-H_2), 6.03 and 6.21 (1H and 1H, each d, *J* = 11.2 Hz, 7- and 6-H); ^{13}C NMR (75 MHz) δ 14.1, 21.9, 22.1, 22.5, 23.3, 23.6, 24.2, 28.2, 28.8, 31.9, 35.2, 40.7, 45.6, 45.9, 47.9, 49.2, 56.5, 67.2, 69.2, 76.2, 112.5, 118.4, 122.2, 135.7, 141.2, 145.1; HRMS (ESI) calcd. for $C_{27}H_{45}O_3$ (M^++ H) 417.3369, measured 417.3374.

4b: $[\alpha]_D^{24}$+17.6 (c 0.9, $CHCl_3$); ^{1}H NMR (300 MHz, $CDCl_3$) δ 0.71 (3H, s, 18-H_3), 0.90 and 0.92 (6H, each d, *J* = 6.6 Hz, 26- and 27-H_3), 1.39 (3H, s, 21-H_3), 2.19 (1H, ddd, *J* = 13.1, 8.7, 4.8 Hz, 1α-H), 2.27 (1H, dd, *J* = 13.1, 7.5 Hz, 4β-H), 2.39 (1H, m, 1β-H), 2.56 (1H, dd, *J* = 13.1, 3.8 Hz, 4α-H), 2.81 (1H, br d, *J* ~ 12 Hz, 9β-H), 3.93 (1H, m, 3α-H), 4.09 (1H, m, 23-H), 4.80 and 5.04 (1H and 1H, each m, 19-H_2), 6.03 and 6.21 (1H and 1H, each d, *J* = 11.2 Hz, 7- and 6-H); ^{13}C NMR (75 MHz) δ 13.8, 21.9, 22.2, 22.4, 23.2, 23.3, 24.3, 26.0, 28.8, 31.9, 35.2, 40.9, 45.9, 46.0, 46.9, 47.4, 56.5, 61.2, 66.8, 69.2, 76.8, 112.5, 118.3, 122.2, 135.6, 141.2, 145.1; HRMS (ESI) calcd. for $C_{27}H_{45}O_3$ (M^++ H) 417.3369, measured 417.3375.

Measurement of CYP27B1 activity on secosteroids

Mouse CYP27B1 was expressed in E. coli and purified as before [68]. CYP27B1 activity was measured on substrate incorporated into the membrane of phospholipid vesicles as described previously [68]. Briefly, phospholipid vesicles were prepared by sonication of dioleoyl phosphatidylcholine, cardiolipin and secosteroid. Vesicles (510 μM phospholipid) were then incubated at 37°C with CYP27B1 (0.2 μM) in buffer comprising 20 mM Hepes, pH 7.4, 100 mM NaCl, 0.1 mM EDTA, 0.1 mM and dithiothreitol, adrenodoxin (15 μM), adrenodoxin reductase (0.4 μM), glucose-6-phosphate (2 mM), glucose-6-phosphate dehydrogenase (2 U/mL) and NAPDH (50 μM) in a volume of 0.5 ml. After reaction (5 or 20 min), the incubation mixture was extracted 3-times with 2.5 ml dichloromethane, extracts combined, dried under N_2 gas and dissolved in 64% methanol. Samples were analysed by reverse phase HPLC on a Grace Alltima column (25 × 0.46 cm) using a gradient of 64 to 100% methanol for 15 min followed by 100% methanol for 30 min, at a flow rate of 0.5 ml/min. Metabolites were detected with a UV detector at 265 nm.

Nuclear receptor analyses

VDR translocation assay—To study the ligand-induced VDR translocation from cytoplasm to the nucleus, we used SKMEL-188 melanoma cells transduced with pLenti-CMV-VDR-EGFP-pgk-puro, which express VDR-GFP fusion protein, and followed the protocols described previously [57, 80, 81]. Briefly, cells were grown on a 96 well plate using Ham's F10 media containing 5% charcoal-treated FBS until 70% confluence. The cells were treated with the secosteroids for 1.5 h in a 96 well plate followed by treatment of NucBlue™ Live ReadyProbes™ Reagent (Invitrogen, Waltham, MA, USA) using the manufacturer's protocol. The ratio of cell number with a fluorescent nucleus (GFP) to the total cell number (DAPI) was determined using Cytation 5 (Biotek, Winooski, VT, USA).

AhR binding assay—The binding of chemically synthesized secosteroids to AhR was tested using the Human AhR Reporter Assay System (Indigo Biosciences, State College, PA, USA) following the manufacturer's protocol and as detailed previously [62]. Briefly, the cells including the luciferase reporter gene linked to an AhR-responsive promoter were treated with the compounds for 23 h and the luminescence signal was measured using Cytation 5 (Biotek, Winooski, VT, USA) after treatment with the detection substrate provided in the kit system.

LXR binding assay—The bindings were performed using the LanthaScreen TR-FRET LXRα/β Coactivator kit (Thermo Fisger Scientific, Inc., Waltham, MA) as described previously [61]. Briefly, TR-FRET ratios were calculated by dividing the emission at 520 nm by that at 495 nm using Synergy neo2 (BioTek, Winooski, VT).

Molecular modeling—To predict binding poses of vitamin D_3 derivatives: 20*S*(OH)D_3, 20*S*,23*S*$(OH)_2D_3$, 20*S*,23*R*$(OH)_2D_3$ and 20*S*,25$(OH)_2D_3$ towards various receptors including VDR, RORα and RORγ, liver X receptors (LXRα and LXRβ) and aryl hydrocarbon receptor (AhR), a receptor-based approach (molecular docking) was used. Crystal structures for VDR (PDBID: 1DB1) [82], RORα (PDBID: 1S0X) [83], RORγ (PDBID: 3L0J) [84], LXRα (PDBID: 5AVI) [85] and LXRβ (PDBID: 5HJP) [86], and a human AhR homology model from our previous study [62] were used for the docking studies. Openbabel [87] software was used to convert the ligands of vitamin D_3 derivatives in PDB format to PDBQT format. Receptors were loaded into AutoDock Tools [88] software for preparation: polar hydrogen atoms were added; water molecules, ion molecules, and bound ATP were removed; and lastly, Kollman Charges were added. Prepared receptors were output in PDBQT format for molecular docking in Autodock Vina [89]. To evaluate the receptor-ligand interaction, 3D and 2D interactions between vitamin D_3 derivatives with each studied receptor were performed using PyMol [90] software for 3D interactions and Maestro [91] for 2D interaction map.

Cell culture studies

Proliferation—Human dermal fibroblasts isolated from the skin of black neonates (HDFn) and human epidermal (HaCaT) keratinocytes cultured as described previously [50, 80] were used for the experiments. Briefly, HDFn were plated onto 96-well plates at a confluence of about 70% in their seventh passage. Both HDFn and HaCaT keratinocytes were treated

with 20*S*(OH)D_3, 20*S*,25(OH)$_2D_3$, 20*S*,23*S*(OH)$_2D_3$, 20*S*,23*R*(OH)$_2D_3$ or 1α,25(OH)$_2D_3$ (Sigma-Aldrich, St. Louis, MO, USA) dissolved in ethanol and diluted in DMEM containing charcoal-treated serum, as previously described [44, 45, 80]. The vehicle control comprised 0.1% ethanol. Proliferation was estimated using MTS (Promega, Madison, WI) assay [44, 45, 80]. The number of viable cells was measured in 6 replicates.

Gene expression—RNA isolation and reverse transcription were performed as described previously [61]. Qantitative RT-PCR was carried out using Sybr green Master Mix (Thermo Scientific, Waltham, MA), in triplicates as previously described [61, 92]. Human epidermal keratinocytes (HEKn) isolated from foreskin of white neonates were cultured until the third passage before treatment as described in the literature [46, 70]. Cells were treated with vitamin D_3 derivatives for 8 h or 24 h and harvested for RNA isolation. Approximately 300 ng of RNA was used for cDNA synthesis and an equal amount of cDNA was used for PCR reactions. Cyclophilin B or GAPDH was used as an internal control. Primers sequences are listed in [45, 81]. Reactions were done in triplicate.

Protein expression—HEKn were cultured until the third passage before treatment. Keratinocytes were plated in a 96-well plate and at 80% confluence, 10^{-7} M secosteroids (or 0.1% ethanol control) were added and cells were incubated for 48 h. Cells were fixed and stained with anti-involucrin (1:20, GTX-14504; Genetex, Irvine, CA, USA) anti-CK10 (1:300, Santa Cruz Biotechnology), anti-catalase (1:200, Santa Cruz Biotechnology) or anti-CK14 antibody with Alexa Fluor® 488 (1:500, Santa Cruz Biotechnology) and imaged at 10× magnification in Cytation 5 reader as described before [45, 81, 93]. Nuclei were stained with blue DAPI. Fluorescence intensity was measured using the Cytation 5 reader and ImageJ, and data were analyzed using Graph Pad Prizm.

Human and T cell activation and analysis—Human peripheral blood mononuclear cells (PBMC) from two healthy individuals were obtained from a pre-existing respository. Their use was approved by the University of Alabama at Birmingham Institutional Review Board (Human Subject Assurance Number FWA00005960) as an exempt protocol #4 (Dr C. Raman, P.I.). The protocol was classified for exempt status under 45CFR46.102 (f) in that is does not involve “human subjects” as defined therein. Informed consent is waived in accord with 45CFR46.116(d). In 48 well plates, 0.5×10^6 PBMC/well were cultured in RPMI1640 containing, 5% charcoal adsorbed FBS and antibiotics and T cells were activated using 0.5 μg/ml anti-CD3 (clone 145–2C11) and 1 μg/ml anti-CD28 (clone 37.51) for 24 h [44, 45, 80, 94, 95]. The culture was treated with 10^{-7} M 20*S*(OH)D_3, 20*S*,25(OH)$_2D_3$, 20*S*,23*S*(OH)$_2D_3$, 20*S*,23*R*(OH)$_2D_3$ or 1α,25(OH)$_2D_3$ (Sigma-Aldrich, St. Louis, MO, USA) dissolved in ethanol and diluted in culture medium at the same time of addition of anti-CD3 and anti-CD28. The vehicle control comprised of 0.1% ethanol. At the end of assay the cells were stained with antibodies to CD4 (clone RPA-T4, BV-421), CD19 (clone HB19, BV-510), CD14 (clone HCD14, Alexa 700), CD137 (clone 4B4–1, BV605), CD8a (clone RPA-T8, FITC), ICOS (clone C398.4A, PE/Dazzle), PD1 (clone NAT105, PE), CD80 (clone 2D10, PerCP/Cy5.5), OX40 (clone ACT35, PE/Cy7), CD69 (clone FN50, APC), HLA-DR (clone L243, APC/Fire 750). All antibodies were from Biolegend except anti-CD8

was from Thermo Fisher. The stained cells were analyzed using a CytoFLEX (Beckman Coulter) flow cytometer.

For unbiased analysis of the multidimensional data, we utilized computational algorithm-based approaches [96]. The flow cytometry standard (FCS) data files from each individual and treatment (two individuals, six treatments including ethanol, a total of 12 data files) were processed through the following workflow – compensation, gating on live cells, gating for single cells and subtraction of $CD19^+$ (B cells) and $CD14^+$ (monocytes). We removed B cells and monocytes from the analysis because only T cells ($CD4^+$ and $CD8^+$) are activated by anti-CD3 and anti-CD28. After these initial gating steps, a key word was added to each of the 12 FCS files, down sampled to 50,000 events/sample and concatenated. Down sampling ascertains that each sample is equally weighted, and concatenation ascertains that statistical analysis is applied equally. The concatenated files were first subjected to TriMAP analysis, a computational algorithm that clusters populations based on triplet relatedness followed by FlowSOM algorithm-based clustering [96]. To perform these analyses, we used the plugins within FlowJo (BD, CA, USA).

Supplementary Material

Refer to Web version on PubMed Central for supplementary material.

Acknowledgement

Supported by grants from NIH grants 1R01AR073004-01A1, R01AR071189-01A1, and a VA merit grant No. 1I01BX004293-01A1 to ATS and R21 AI152047-01A1 to RC and ATS.

References:

[1]. Holick MF, MacLaughlin JA, Doppelt SH, Regulation of cutaneous previtamin D_3 photosynthesis in man: skin pigment is not an essential regulator, Science 211(4482) (1981) 590–3. [PubMed: 6256855]

[2]. Holick MF, Tian XQ, Allen M, Evolutionary importance for the membrane enhancement of the production of vitamin D_3 in the skin of poikilothermic animals, Proc Natl Acad Sci U S A 92(8) (1995) 3124–6. [PubMed: 7724526]

[3]. Bikle DD, Vitamin D: an ancient hormone, Exp Dermatol 20(1) (2011) 7–13. [PubMed: 21197695]

[4]. Bikle DD, Vitamin D: newly discovered actions require reconsideration of physiologic requirements, Trends Endocrinol Metab 21(6) (2010) 375–84. [PubMed: 20149679]

[5]. Holick MF, Vitamin D: A millenium perspective, J Cell Biochem 88(2) (2003) 296–307. [PubMed: 12520530]

[6]. Jenkinson C, The vitamin D metabolome: An update on analysis and function, Cell Biochem Funct (2019).

[7]. Tuckey RC, Cheng CYS, Slominski AT, The serum vitamin D metabolome: What we know and what is still to discover, J Steroid Biochem Mol Biol 186 (2019) 4–21. [PubMed: 30205156]

[8]. Bikle DD, Vitamin D receptor, UVR, and skin cancer: a potential protective mechanism, J Invest Dermatol 128(10) (2008) 2357–61. [PubMed: 18787544]

[9]. Bikle DD, Vitamin D metabolism and function in the skin, Mol Cell Endocrinol 347(1–2) (2011) 80–9. [PubMed: 21664236]

[10]. Holick MF, Vitamin D deficiency, N Engl J Med 357(3) (2007) 266–81. [PubMed: 17634462]

[11]. Plum LA, DeLuca HF, Vitamin D, disease and therapeutic opportunities, Nature reviews. Drug discovery 9(12) (2010) 941–55. [PubMed: 21119732]

[12]. Bikle DD, Vitamin D: Newer Concepts of Its Metabolism and Function at the Basic and Clinical Level, J Endocr Soc 4(2) (2020) bvz038. [PubMed: 32051922]

[13]. Carlberg C, Vitamin D Genomics: From In Vitro to In Vivo, Front Endocrinol (Lausanne) 9 (2018) 250. [PubMed: 29875733]

[14]. Zmijewski MA, Carlberg C, Vitamin D receptor(s): In the nucleus but also at membranes?, Exp Dermatol (2020).

[15]. Bouillon R, Marcocci C, Carmeliet G, Bikle D, White JH, Dawson-Hughes B, Lips P, Munns CF, Lazaretti-Castro M, Giustina A, Bilezikian J, Skeletal and Extraskeletal Actions of Vitamin D: Current Evidence and Outstanding Questions, Endocrine Reviews 40(4) (2018) 1109–1151.

[16]. Slominski AT, Brozyna AA, Zmijewski MA, Jozwicki W, Jetten AM, Mason RS, Tuckey RC, Elmets CA, Vitamin D signaling and melanoma: role of vitamin D and its receptors in melanoma progression and management, Lab Invest 97(6) (2017) 706–724. [PubMed: 28218743]

[17]. Hewison M, An update on vitamin D and human immunity, Clinical Endocrinology 76(3) (2012) 315–325. [PubMed: 21995874]

[18]. Suaini NHA, Zhang Y, Vuillermin PJ, Allen KJ, Harrison LC, Immune Modulation by Vitamin D and Its Relevance to Food Allergy, Nutrients 7(8) (2015) 6088–6108. [PubMed: 26225992]

[19]. Bikle DD, Vitamin D and the skin: Physiology and pathophysiology, Rev Endocr Metab Disord 13(1) (2012) 3–19. [PubMed: 21845365]

[20]. Reichrath J, Saternus R, Vogt T, Endocrine actions of vitamin D in skin: Relevance for photocarcinogenesis of non-melanoma skin cancer, and beyond, Mol Cell Endocrinol 453 (2017) 96–102. [PubMed: 28526240]

[21]. Grant WB, Roles of Solar UVB and Vitamin D in Reducing Cancer Risk and Increasing Survival, Anticancer research 36(3) (2016) 1357–70. [PubMed: 26977037]

[22]. Chang SH, Chung Y, Dong C, Vitamin D Suppresses Th17 Cytokine Production by Inducing C/EBP Homologous Protein (CHOP) Expression, Journal of Biological Chemistry 285(50) (2010) 38751–38755.

[23]. Szodoray P, Nakken B, Gaal J, Jonsson R, Szegedi A, Zold E, Szegedi G, Brun JG, Gesztelyi R, Zeher M, Bodolay E, The complex role of vitamin D in autoimmune diseases, Scandinavian journal of immunology 68(3) (2008) 261–9. [PubMed: 18510590]

[24]. Daniel C, Sartory NA, Zahn N, Radeke HH, Stein JM, Immune Modulatory Treatment of Trinitrobenzene Sulfonic Acid Colitis with Calcitriol Is Associated with a Change of a T Helper (Th) 1/Th17 to a Th2 and Regulatory T Cell Profile, Journal of Pharmacology and Experimental Therapeutics 324(1) (2008) 23–33.

[25]. Wöbke TK, Sorg BL, Steinhilber D, Vitamin D in inflammatory diseases, Frontiers in Physiology 5 (2014) 244. [PubMed: 25071589]

[26]. Chun RF, Liu PT, Modlin RL, Adams JS, Hewison M, Impact of vitamin D on immune function: lessons learned from genome-wide analysis, Frontiers in Physiology 5 (2014) 151. [PubMed: 24795646]

[27]. Rossini M, Maddali Bongi S, La Montagna G, Minisola G, Malavolta N, Bernini L, Cacace E, Sinigaglia L, Di Munno O, Adami S, Vitamin D deficiency in rheumatoid arthritis: prevalence, determinants and associations with disease activity and disability, Arthritis research & therapy 12(6) (2010) R216. [PubMed: 21114806]

[28]. Palm NW, Rosenstein RK, Medzhitov R, Allergic host defences, Nature 484(7395) (2012) 465–472. [PubMed: 22538607]

[29]. Ikeda U, Wakita D, Ohkuri T, Chamoto K, Kitamura H, Iwakura Y, Nishimura T, 1α,25-Dihydroxyvitamin D_3 and all-trans retinoic acid synergistically inhibit the differentiation and expansion of Th17 cells, Immunology Letters 134(1) (2010) 7–16. [PubMed: 20655952]

[30]. Mayne CG, Spanier JA, Relland LM, Williams CB, Hayes CE, 1,25-Dihydroxyvitamin D3 acts directly on the T lymphocyte vitamin D receptor to inhibit experimental autoimmune encephalomyelitis, European Journal of Immunology 41(3) (2011) 822–832. [PubMed: 21287548]

[31]. Hartmann B, Riedel R, Jors K, Loddenkemper C, Steinmeyer A, Zugel U, Babina M, Radbruch A, Worm M, Vitamin D Receptor Activation Improves Allergen-Triggered Eczema in Mice, J Invest Dermatol 132(2) (2012) 330–336. [PubMed: 21938012]

[32]. Slominski AT, Janjetovic Z, Fuller BE, Zmijewski MA, Tuckey RC, Nguyen MN, Sweatman T, Li W, Zjawiony J, Miller D, Chen TC, Lozanski G, Holick MF, Products of vitamin D_3 or 7-dehydrocholesterol metabolism by cytochrome P450scc show anti-leukemia effects, having low or absent calcemic activity, PloS one 5(3) (2010) e9907. [PubMed: 20360850]

[33]. Wang J, Slominski A, Tuckey RC, Janjetovic Z, Kulkarni A, Chen J, Postlethwaite AE, Miller D, Li W, 20-hydroxyvitamin D_3 inhibits proliferation of cancer cells with high efficacy while being non-toxic, Anticancer research 32(3) (2012) 739–46. [PubMed: 22399586]

[34]. Biankin AV, Waddell N, Kassahn KS, Gingras M-C, Muthuswamy LB, Johns AL, Miller DK, Wilson PJ, Patch A-M, Wu J, Chang DK, Cowley MJ, Gardiner BB, Song S, Harliwong I, Idrisoglu S, Nourse C, Nourbakhsh E, Manning S, Wani S, Gongora M, Pajic M, Scarlett CJ, Gill AJ, Pinho AV, Rooman I, Anderson M, Holmes O, Leonard C, Taylor D, Wood S, Xu Q, Nones K, Lynn Fink J, Christ A, Bruxner T, Cloonan N, Kolle G, Newell F, Pinese M, Scott Mead R, Humphris JL, Kaplan W, Jones MD, Colvin EK, Nagrial AM, Humphrey ES, Chou A, Chin VT, Chantrill LA, Mawson A, Samra JS, Kench JG, Lovell JA, Daly RJ, Merrett ND, Toon C, Epari K, Nguyen NQ, Barbour A, Zeps N, Kakkar N, Zhao F, Qing Wu Y, Wang M, Muzny DM, Fisher WE, Charles Brunicardi F, Hodges SE, Reid JG, Drummond J, Chang K, Han Y, Lewis LR, Dinh H, Buhay CJ, Beck T, Timms L, Sam M, Begley K, Brown A, Pai D, Panchal A, Buchner N, De Borja R, Denroche RE, Yung CK, Serra S, Onetto N, Mukhopadhyay D, Tsao M-S, Shaw PA, Petersen GM, Gallinger S, Hruban RH, Maitra A, Iacobuzio-Donahue CA, Schulick RD, Wolfgang CL, Morgan RA, Lawlor RT, Capelli P, Corbo V, Scardoni M, Tortora G, Tempero MA, Mann KM, Jenkins NA, Perez-Mancera PA, Adams DJ, Largaespada DA, Wessels LFA, Rust AG, Stein LD, Tuveson DA, Copeland NG, Musgrove EA, Scarpa A, Eshleman JR, Hudson TJ, Sutherland RL, Wheeler DA, Pearson JV, McPherson JD, Gibbs RA, Grimmond SM, Pancreatic cancer genomes reveal aberrations in axon guidance pathway genes, Nature 491(7424) (2012) 399–405. [PubMed: 23103869]

[35]. Slominski AT, Li W, Kim TK, Semak I, Wang J, Zjawiony JK, Tuckey RC, Novel activities of CYP11A1 and their potential physiological significance, J Steroid Biochem Mol Biol 151 (2015) 25–37. [PubMed: 25448732]

[36]. Tuckey RC, Li W, Zjawiony JK, Zmijewski MA, Nguyen MN, Sweatman T, Miller D, Slominski A, Pathways and products for the metabolism of vitamin D_3 by cytochrome P450scc, The FEBS journal 275(10) (2008) 2585–96. [PubMed: 18410379]

[37]. Slominski RM, Raman C, Elmets C, Jetten AM, Slominski A, Tuckey RC, The significance of CYP11A1 expression in skin physiology and pathology, Mol Cell Endocrinol Available online 12 March 2021, 111238 (2021) 111238. [PubMed: 33716049]

[38]. Slominski AT, Kim TK, Shehabi HZ, Semak I, Tang EK, Nguyen MN, Benson HA, Korik E, Janjetovic Z, Chen J, Yates CR, Postlethwaite A, Li W, Tuckey RC, In vivo evidence for a novel pathway of vitamin D_3 metabolism initiated by P450scc and modified by CYP27B1, FASEB J 26(9) (2012) 3901–15. [PubMed: 22683847]

[39]. Slominski AT, Kim TK, Li W, Tuckey RC, Classical and non-classical metabolic transformation of vitamin D in dermal fibroblasts, Exp Dermatol 25(3) (2016) 231–2. [PubMed: 26440881]

[40]. Slominski AT, Kim TK, Li W, Postlethwaite A, Tieu EW, Tang EK, Tuckey RC, Detection of novel CYP11A1-derived secosteroids in the human epidermis and serum and pig adrenal gland, Sci Rep 5 (2015) 14875. [PubMed: 26445902]

[41]. Jenkinson C, Desai R, Slominski AT, Tuckey RC, Hewison M, Handelsman DJ, Simultaneous measurement of 13 circulating vitamin D3 and D2 mono and dihydroxy metabolites using liquid chromatography mass spectrometry, Clin Chem Lab Med (2021).

[42]. Kim TK, Atigadda V, Brzeminski P, Fabisiak A, Tang EKY, Tuckey RC, Slominski AT, Detection of 7-Dehydrocholesterol and Vitamin D3 Derivatives in Honey, Molecules 25(11) (2020).

[43]. Slominski AT, Chaiprasongsuk A, Janjetovic Z, Kim TK, Stefan J, Slominski RM, Hanumanthu VS, Raman C, Qayyum S, Song Y, Song Y, Panich U, Crossman DK, Athar M, Holick MF, Jetten AM, Zmijewski MA, Zmijewski J, Tuckey RC, Photoprotective Properties of Vitamin D

and Lumisterol Hydroxyderivatives, Cell Biochem Biophys 78(2) (2020) 165–180. [PubMed: 32441029]

[44]. Janjetovic Z, Postlethwaite A, Kang HS, Kim TK, Tuckey RC, Crossman DK, Qayyum S, Jetten AM, Slominski AT, Antifibrogenic Activities of CYP11A1-derived Vitamin D3-hydroxyderivatives Are Dependent on RORgamma, Endocrinology 162(1) (2021).

[45]. Chaiprasongsuk A, Janjetovic Z, Kim TK, Tuckey RC, Li W, Raman C, Panich U, Slominski AT, CYP11A1-derived vitamin D_3 products protect against UVB-induced inflammation and promote keratinocytes differentiation, Free Radic Biol Med 155 (2020) 87–98. [PubMed: 32447000]

[46]. Chaiprasongsuk A, Janjetovic Z, Kim TK, Jarrett SG, D'Orazio JA, Holick MF, Tang EKY, Tuckey RC, Panich U, Li W, Slominski AT, Protective effects of novel derivatives of vitamin D3 and lumisterol against UVB-induced damage in human keratinocytes involve activation of Nrf2 and p53 defense mechanisms, Redox Biol 24 (2019) 101206. [PubMed: 31039479]

[47]. Slominski AT, Brozyna AA, Zmijewski MA, Janjetovic Z, Kim TK, Slominski RM, Tuckey RC, Mason RS, Jetten AM, Guroji P, Reichrath J, Elmets C, Athar M, The role of classical and novel forms of vitamin D in the pathogenesis and progression of non-melanoma skin cancers, Advances in Experimental Medicine and Biology in press (2020).

[48]. Slominski AT, Kim TK, Li W, Yi AK, Postlethwaite A, Tuckey RC, The role of CYP11A1 in the production of vitamin D metabolites and their role in the regulation of epidermal functions, J Steroid Biochem Mol Biol 144PA (2014) 28–39.

[49]. Janjetovic Z, Tuckey RC, Nguyen MN, Thorpe EM Jr., Slominski AT, 20,23-dihydroxyvitamin D3, novel P450scc product, stimulates differentiation and inhibits proliferation and NF-kappaB activity in human keratinocytes, Journal of cellular physiology 223(1) (2010) 36–48. [PubMed: 20020487]

[50]. Slominski A, Janjetovic Z, Tuckey RC, Nguyen MN, Bhattacharya KG, Wang J, Li W, Jiao Y, Gu W, Brown M, Postlethwaite AE, 20S-hydroxyvitamin D_3, noncalcemic product of CYP11A1 action on vitamin D_3, exhibits potent antifibrogenic activity in vivo, The Journal of clinical endocrinology and metabolism 98(2) (2013) E298–303. [PubMed: 23295467]

[51]. Slominski AT, Kim TK, Li W, Yi AK, Postlethwaite A, Tuckey RC, The role of CYP11A1 in the production of vitamin D metabolites and their role in the regulation of epidermal functions, J Steroid Biochem Mol Biol 144 Pt A (2014) 28–39. [PubMed: 24176765]

[52]. Podgorska E, Kim TK, Janjetovic Z, Urbanska K, Tuckey RC, Bae S, Slominski AT, Knocking out the Vitamin D Receptor Enhances Malignancy and Decreases Responsiveness to Vitamin D3 Hydroxyderivatives in Human Melanoma Cells, Cancers (Basel) 13(13) (2021).

[53]. Tieu EW, Tang EK, Chen J, Li W, Nguyen MN, Janjetovic Z, Slominski A, Tuckey RC, Rat CYP24A1 acts on 20-hydroxyvitamin D_3 producing hydroxylated products with increased biological activity, Biochem Pharmacol 84(12) (2012) 1696–704. [PubMed: 23041230]

[54]. Tongkao-On W, Carter S, Reeve VE, Dixon KM, Gordon-Thomson C, Halliday GM, Tuckey RC, Mason RS, CYP11A1 in skin: an alternative route to photoprotection by vitamin D compounds, J Steroid Biochem Mol Biol 148 (2015) 72–8. [PubMed: 25448743]

[55]. Skobowiat C, Oak AS, Kim TK, Yang CH, Pfeffer LM, Tuckey RC, Slominski AT, Noncalcemic 20-hydroxyvitamin D_3 inhibits human melanoma growth in in vitro and in vivo models, Oncotarget 8(6) (2017) 9823–9834. [PubMed: 28039464]

[56]. Chen J, Wang J, Kim TK, Tieu EW, Tang EK, Lin Z, Kovacic D, Miller DD, Postlethwaite A, Tuckey RC, Slominski AT, Li W, Novel vitamin D analogs as potential therapeutics: metabolism, toxicity profiling, and antiproliferative activity, Anticancer research 34(5) (2014) 2153–63. [PubMed: 24778017]

[57]. Kim TK, Wang J, Janjetovic Z, Chen J, Tuckey RC, Nguyen MN, Tang EK, Miller D, Li W, Slominski AT, Correlation between secosteroid-induced vitamin D receptor activity in melanoma cells and computer-modeled receptor binding strength, Mol Cell Endocrinol 361(1–2) (2012) 143–52. [PubMed: 22546549]

[58]. Slominski AT, Kim TK, Hobrath JV, Oak ASW, Tang EKY, Tieu EW, Li W, Tuckey RC, Jetten AM, Endogenously produced nonclassical vitamin D hydroxy-metabolites act as "biased" agonists on VDR and inverse agonists on RORalpha and RORgamma, J Steroid Biochem Mol Biol 173 (2017) 42–56. [PubMed: 27693422]

[59]. Lin Z, Marepally SR, Goh ESY, Cheng CYS, Janjetovic Z, Kim TK, Miller DD, Postlethwaite AE, Slominski AT, Tuckey RC, Peluso-Iltis C, Rochel N, Li W, Investigation of 20S-hydroxyvitamin D_3 analogs and their 1alpha-OH derivatives as potent vitamin D receptor agonists with anti-inflammatory activities, Sci Rep 8(1) (2018) 1478. [PubMed: 29367669]

[60]. Slominski AT, Kim TK, Takeda Y, Janjetovic Z, Brozyna AA, Skobowiat C, Wang J, Postlethwaite A, Li W, Tuckey RC, Jetten AM, RORalpha and ROR gamma are expressed in human skin and serve as receptors for endogenously produced noncalcemic 20-hydroxy- and 20,23-dihydroxyvitamin D, FASEB J 28(7) (2014) 2775–89. [PubMed: 24668754]

[61]. Slominski AT, Kim TK, Qayyum S, Song Y, Janjetovic Z, Oak ASW, Slominski RM, Raman C, Stefan J, Mier-Aguilar CA, Atigadda V, Crossman DK, Golub A, Bilokin Y, Tang EKY, Chen JY, Tuckey RC, Jetten AM, Song Y, Vitamin D and lumisterol derivatives can act on liver X receptors (LXRs), Sci Rep 11(1) (2021) 8002. [PubMed: 33850196]

[62]. Slominski AT, Kim TK, Janjetovic Z, Brozyna AA, Zmijewski MA, Xu H, Sutter TR, Tuckey RC, Jetten AM, Crossman DK, Differential and Overlapping Effects of $20,23(OH)_2D_3$ and $1,25(OH)_2D_3$ on Gene Expression in Human Epidermal Keratinocytes: Identification of AhR as an Alternative Receptor for $20,23(OH)_2D_3$, Int J Mol Sci 19(10) (2018).

[63]. Li W, Chen J, Janjetovic Z, Kim TK, Sweatman T, Lu Y, Zjawiony J, Tuckey RC, Miller D, Slominski A, Chemical synthesis of 20S-hydroxyvitamin D_3, which shows antiproliferative activity, Steroids 75(12) (2010) 926–35. [PubMed: 20542050]

[64]. Sibilska-Kaminski IK, Sicinski RR, Plum LA, DeLuca HF, Synthesis and Biological Activity of 2,22-Dimethylene Analogues of 19-Norcalcitriol and Related Compounds, J Med Chem 63(13) (2020) 7355–7368. [PubMed: 32510210]

[65]. Wang Q, Lin Z, Kim TK, Slominski AT, Miller DD, Li W, Total synthesis of biologically active 20S-hydroxyvitamin D_3, Steroids 104 (2015) 153–62. [PubMed: 26433048]

[66]. Tang EK, Chen J, Janjetovic Z, Tieu EW, Slominski AT, Li W, Tuckey RC, Hydroxylation of CYP11A1-derived products of vitamin D_3 metabolism by human and mouse CYP27B1, Drug metabolism and disposition: the biological fate of chemicals 41(5) (2013) 1112–24. [PubMed: 23454830]

[67]. Lin Z, Marepally SR, Ma D, Kim TK, Oak AS, Myers LK, Tuckey RC, Slominski AT, Miller DD, Li W, Synthesis and Biological Evaluation of Vitamin D_3 Metabolite 20S,23S-Dihydroxyvitamin D3 and Its 23R Epimer, J Med Chem 59(10) (2016) 5102–8. [PubMed: 27070779]

[68]. Tang EK, Li W, Janjetovic Z, Nguyen MN, Wang Z, Slominski A, Tuckey RC, Purified mouse CYP27B1 can hydroxylate 20,23-dihydroxyvitamin D_3, producing 1alpha,20,23-trihydroxyvitamin D_3, which has altered biological activity, Drug metabolism and disposition: the biological fate of chemicals 38(9) (2010) 1553–9. [PubMed: 20554701]

[69]. Zbytek B, Janjetovic Z, Tuckey RC, Zmijewski MA, Sweatman TW, Jones E, Nguyen MN, Slominski AT, 20-Hydroxyvitamin D_3, a product of vitamin D_3 hydroxylation by cytochrome P450scc, stimulates keratinocyte differentiation, J Invest Dermatol 128(9) (2008) 2271–80. [PubMed: 18368131]

[70]. Janjetovic Z, Zmijewski MA, Tuckey RC, DeLeon DA, Nguyen MN, Pfeffer LM, Slominski AT, 20-Hydroxycholecalciferol, product of vitamin D3 hydroxylation by P450scc, decreases NF-kappaB activity by increasing IkappaB alpha levels in human keratinocytes, PloS one 4(6) (2009) e5988. [PubMed: 19543524]

[71]. Slominski AT, Janjetovic Z, Kim TK, Wright AC, Grese LN, Riney SJ, Nguyen MN, Tuckey RC, Novel vitamin D hydroxyderivatives inhibit melanoma growth and show differential effects on normal melanocytes, Anticancer research 32(9) (2012) 3733–42. [PubMed: 22993313]

[72]. Brozyna AA, Kim TK, Zablocka M, Jozwicki W, Yue J, Tuckey RC, Jetten AM, Slominski AT, Association among Vitamin D, Retinoic Acid-Related Orphan Receptors, and Vitamin D Hydroxyderivatives in Ovarian Cancer, Nutrients 12(11) (2020).

[73]. Slominski AT, Janjetovic Z, Kim TK, Wasilewski P, Rosas S, Hanna S, Sayre RM, Dowdy JC, Li W, Tuckey RC, Novel non-calcemic secosteroids that are produced by human epidermal keratinocytes protect against solar radiation, J Steroid Biochem Mol Biol 148 (2015) 52–63. [PubMed: 25617667]

[74]. Slominski AT, Brozyna AA, Skobowiat C, Zmijewski MA, Kim TK, Janjetovic Z, Oak AS, Jozwicki W, Jetten AM, Mason RS, Elmets C, Li W, Hoffman RM, Tuckey RC, On the role of classical and novel forms of vitamin D in melanoma progression and management, J Steroid Biochem Mol Biol 177 (2018) 159–170. [PubMed: 28676457]

[75]. Lin Z, Chen H, Belorusova AY, Bollinger JC, Tang EKY, Janjetovic Z, Kim TK, Wu Z, Miller DD, Slominski AT, Postlethwaite AE, Tuckey RC, Rochel N, Li W, 1alpha,20S-Dihydroxyvitamin D3 Interacts with Vitamin D Receptor: Crystal Structure and Route of Chemical Synthesis, Sci Rep 7(1) (2017) 10193. [PubMed: 28860545]

[76]. Boppana S, Qin K, Files JK, Russell RM, Stoltz R, Bibollet-Ruche F, Bansal A, Erdmann N, Hahn BH, Goepfert PA, SARS-CoV-2-specific circulating T follicular helper cells correlate with neutralizing antibodies and increase during early convalescence, PLoS Pathog 17(7) (2021) e1009761. [PubMed: 34270631]

[77]. Grifoni A, Sidney J, Vita R, Peters B, Crotty S, Weiskopf D, Sette A, SARS-CoV-2 human T cell epitopes: Adaptive immune response against COVID-19, Cell Host Microbe 29(7) (2021) 1076–1092. [PubMed: 34237248]

[78]. Anchang B, Hart TD, Bendall SC, Qiu P, Bjornson Z, Linderman M, Nolan GP, Plevritis SK, Visualization and cellular hierarchy inference of single-cell data using SPADE, Nat Protoc 11(7) (2016) 1264–79. [PubMed: 27310265]

[79]. Palit S, Heuser C, de Almeida GP, Theis FJ, Zielinski CE, Meeting the Challenges of High-Dimensional Single-Cell Data Analysis in Immunology, Front Immunol 10 (2019) 1515. [PubMed: 31354705]

[80]. Slominski AT, Kim TK, Janjetovic Z, Tuckey RC, Bieniek R, Yue J, Li W, Chen J, Nguyen MN, Tang EK, Miller D, Chen TC, Holick M, 20-Hydroxyvitamin D_2 is a noncalcemic analog of vitamin D with potent antiproliferative and prodifferentiation activities in normal and malignant cells, Am J Physiol Cell Physiol 300(3) (2011) C526–41. [PubMed: 21160030]

[81]. Slominski AT, Kim TK, Hobrath JV, Janjetovic Z, Oak ASW, Postlethwaite A, Lin Z, Li W, Takeda Y, Jetten AM, Tuckey RC, Characterization of a new pathway that activates lumisterol in vivo to biologically active hydroxylumisterols, Sci Rep 7(1) (2017) 11434. [PubMed: 28900196]

[82]. Rochel N, Wurtz J, Mitschler A, Klaholz B, Moras D, The crystal structure of the nuclear receptor for vitamin D bound to its natural ligand, Molecular cell 5(1) (2000) 173–179. [PubMed: 10678179]

[83]. Kallen J, Schlaeppi J-M, Bitsch F, Delhon I, Fournier B, Crystal structure of the human RORα ligand binding domain in complex with cholesterol sulfate at 2.2 Å, Journal of Biological Chemistry 279(14) (2004) 14033–14038.

[84]. Jin L, Martynowski D, Zheng S, Wada T, Xie W, Li Y, Structural basis for hydroxycholesterols as natural ligands of orphan nuclear receptor RORγ, Molecular endocrinology 24(5) (2010) 923–929. [PubMed: 20203100]

[85]. Matsui Y, Yamaguchi T, Yamazaki T, Yoshida M, Arai M, Terasaka N, Honzumi S, Wakabayashi K, Hayashi S, Nakai D, Discovery and structure-guided optimization of tert-butyl 6-(phenoxymethyl)-3-(trifluoromethyl) benzoates as liver X receptor agonists, Bioorganic & medicinal chemistry letters 25(18) (2015) 3914–3920. [PubMed: 26238323]

[86]. Stachel SJ, Zerbinatti C, Rudd MT, Cosden M, Suon S, Nanda KK, Wessner K, DiMuzio J, Maxwell J, Wu Z, Identification and in vivo evaluation of liver X receptor β-selective agonists for the potential treatment of Alzheimer's disease, Journal of medicinal chemistry 59(7) (2016) 3489–3498. [PubMed: 27011007]

[87]. O'Boyle NM, Banck M, James CA, Morley C, Vandermeersch T, Hutchison GR, Open Babel: An open chemical toolbox, Journal of Cheminformatics 3(1) (2011) 33. [PubMed: 21982300]

[88]. Morris GM, Huey R, Lindstrom W, Sanner MF, Belew RK, Goodsell DS, Olson AJ, AutoDock4 and AutoDockTools4: Automated docking with selective receptor flexibility, Journal of computational chemistry 30(16) (2009) 2785–91. [PubMed: 19399780]

[89]. Trott O, Olson AJ, AutoDock Vina: Improving the speed and accuracy of docking with a new scoring function, efficient optimization, and multithreading, Journal of Computational Chemistry 31(2) (2010) 455–461. [PubMed: 19499576]

[90]. Schrodinger, LLC, The PyMOL Molecular Graphics System, Version 1.8, 2015.

[91]. Maestro, Schrödinger, LLC, New York, NY, 2020.

[92]. Janjetovic Z, Nahmias ZP, Hanna S, Jarrett SG, Kim TK, Reiter RJ, Slominski AT, Melatonin and its metabolites ameliorate ultraviolet B-induced damage in human epidermal keratinocytes, J Pineal Res 57(1) (2014) 90–102. [PubMed: 24867336]

[93]. Chaiprasongsuk A, Janjetovic Z, Kim TK, Schwartz CJ, Tuckey RC, Tang EKY, Raman C, Panich U, Slominski AT, Hydroxylumisterols, Photoproducts of Pre-Vitamin D_3, Protect Human Keratinocytes against UVB-Induced Damage, Int J Mol Sci 21(24) (2020).

[94]. McGuire DJ, Rowse AL, Li H, Peng BJ, Sestero CM, Cashman KS, De Sarno P, Raman C, CD5 enhances Th17-cell differentiation by regulating IFN-gamma response and RORgammat localization, Eur J Immunol 44(4) (2014) 1137–42. [PubMed: 24356888]

[95]. Sestero CM, McGuire DJ, De Sarno P, Brantley EC, Soldevila G, Axtell RC, Raman C, CD5-dependent CK2 activation pathway regulates threshold for T cell anergy, J Immunol 189(6) (2012) 2918–30. [PubMed: 22904299]

[96]. Quintelier K, Couckuyt A, Emmaneel A, Aerts J, Saeys Y, Van Gassen S, Analyzing high-dimensional cytometry data using FlowSOM, Nature Protocols 16(8) (2021) 3775–3801. [PubMed: 34172973]

Highlights

- more efficient routes of chemical synthesis for 20*S*(OH)D_3, 20*S*,23*S*$(OH)_2D_3$, 20*S*,23*R*$(OH)_2D_3$ are reported
- new synthetic pathway for 20*S*,25$(OH)_2D_3$ is reported
- phenotypic effects of D3 derivatives are compared
- actions of D3 derivatives on different nuclear receptors are compared
- analysis of D3 derivatives on T cell activation in PBMC is reported

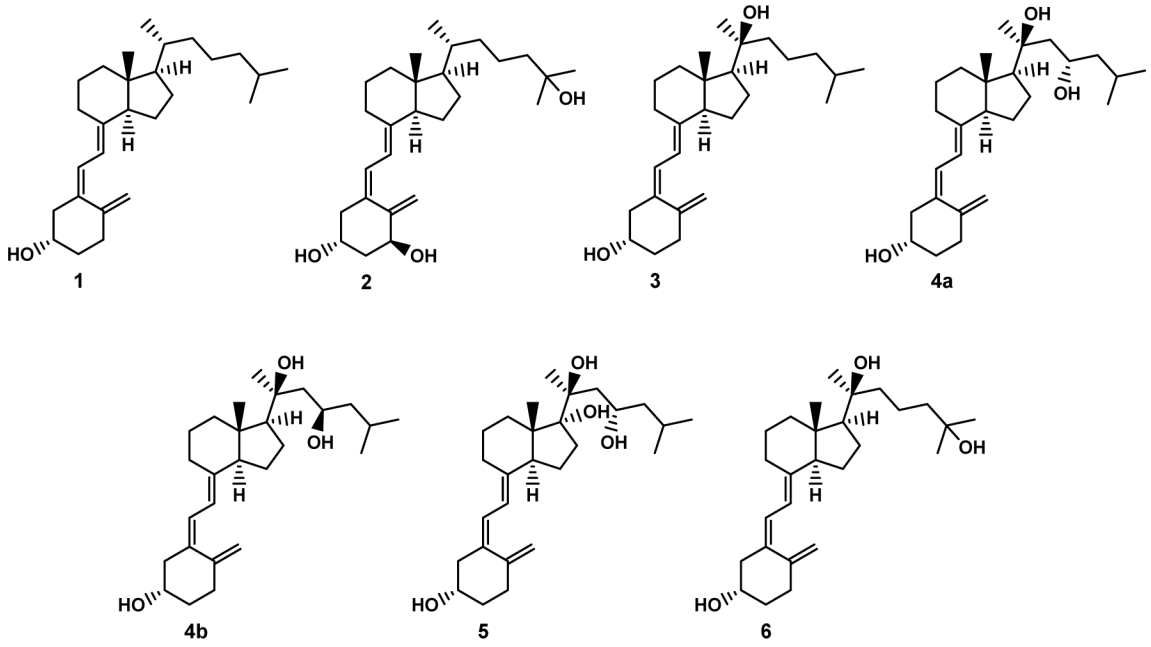

Figure 1.
Chemical structure of vitamin D_3 and some of its biologically important derivatives.

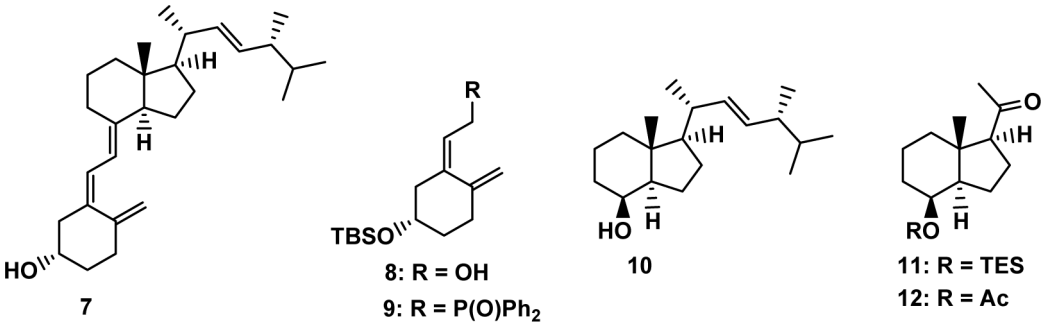

Figure 2.

Vitamin D_2 (**7**) and the building blocks used as the key intermediates in the synthesis of target vitamin D compounds.

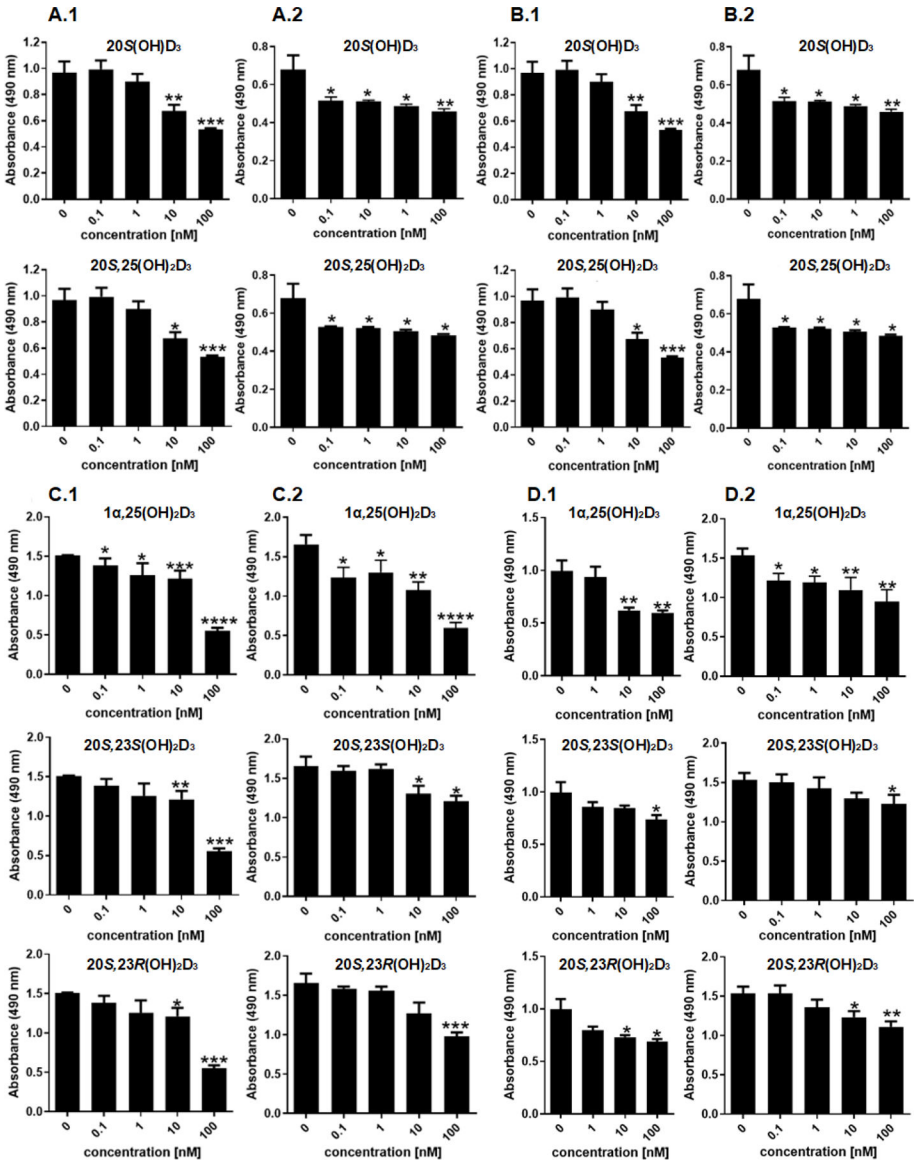

Figure 3.

Inhibition of cell proliferation by 20*S*(OH)D_3, 20*S*,25$(OH)_2D_3$, 20*S*,23*S*$(OH)_2D_3$ and 20*S*,23*R*$(OH)_2D_3$ in comparison to 1α,25$(OH)_2D_3$. Human epidermal (HaCaT) keratinocytes (A, C) or dermal fibroblasts (B, D) were treated for 24 h (1) or 48 h (2) with graded concentrations of the compounds: 0.1, 1, 10, or 100 nM. Ethanol (0.1%) served as a negative control. Data are means ± SD (n = 6) and were analyzed using Student's *t*-test with $p < 0.05$ (*), $p < 0.01$ (**) or $p < 0.001$ (***).

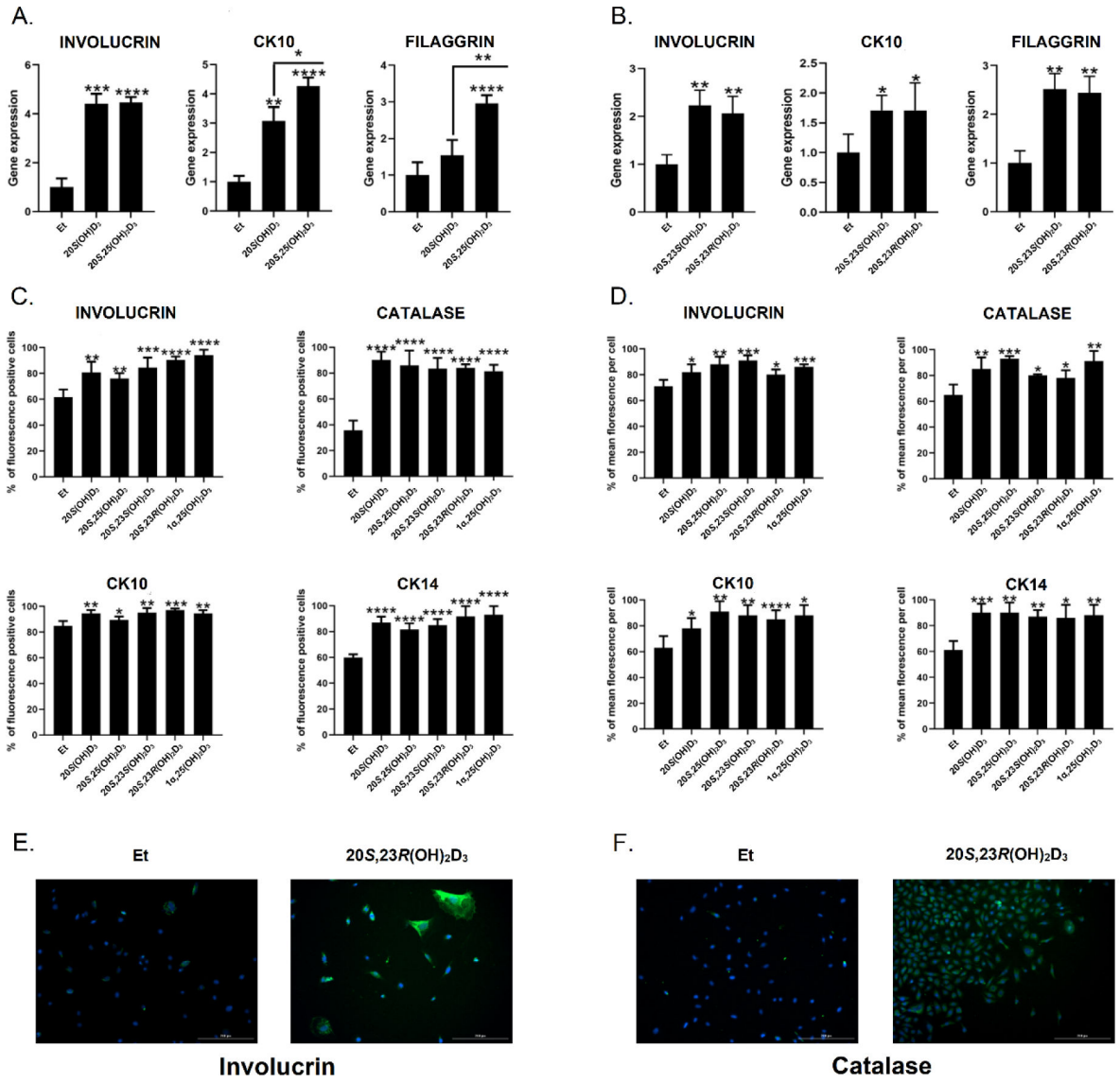

Figure 4.

Stimulation of keratinocyte differentiation by 20*S*(OH)D_3, 20*S*,25$(OH)_2D_3$, 20*S*,23*S*$(OH)_2D_3$ and 20*S*,23*R*$(OH)_2D_3$ in comparison to 1α,25$(OH)_2D_3$. Human neonatal epidermal keratinocytes were treated for 8 (A), 24 h (B) or 48 h (C, D) with 0.1, 1, 10, or 100 nM secosteroid or 0.1% ethanol (negative control). A and B: relative gene expression studies with cyclophilin B used as internal control and presented as fold change vs vehicle control. C, D: protein expression studies. Values are presented as percentage of fluorescence positive cells (C) or as mean fluorescence per cell (% of all cells (D). The values in D were calculated as mean green fluorescence vs DAPI blue fluorescence measured in ImageJ. E, F: Representative fluorescence (green) of cells stained with antibodies against involucrin (E) or catalase (F). Nuclei (blue) are stained with DAPI. Data are means ± SD (n = 3) and were analyzed using Student's *t*-test with $p < 0.05$ (*), $p < 0.01$ (**) or $p < 0.001$ (***).

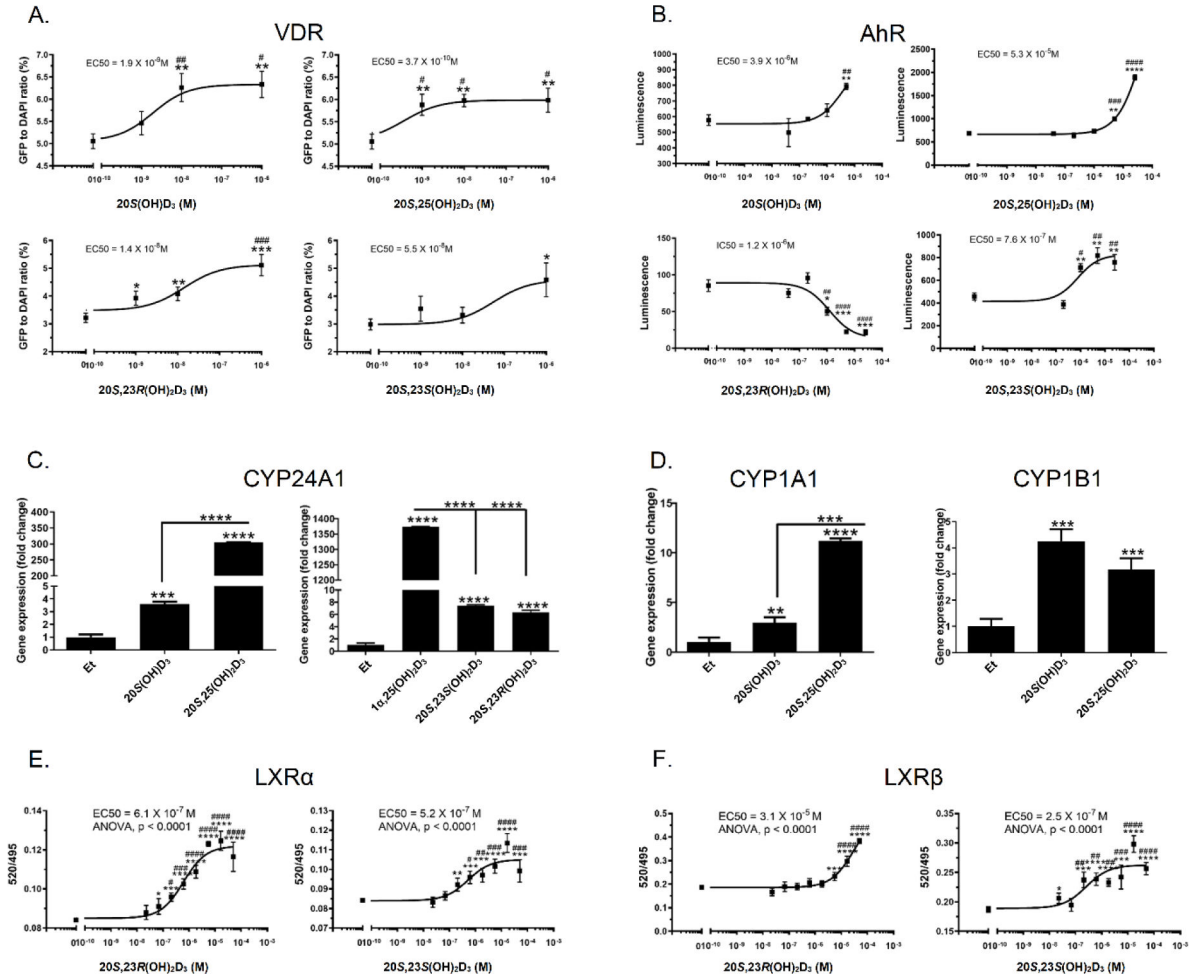

Figure 5.

Interaction of 20*S*(OH)D_3, 20*S*,25(OH)$_2D_3$, 20*S*,23*S*(OH)$_2D_3$ and 20*S*,23*R*(OH)$_2D_3$ with nuclear receptors. A: ligand induced translocation of the VDR-GFP from the cytoplasm to nucleus. B: stimulation of AhR binding activity by secosteroids using AhR Reporter Cells including the luciferase reporter gene linked to an AhR-responsive promoter (Indigo Biosciences, State College, PA). C: ligand induced stimulation of CYP24A1 gene expression after 8 h of incubation. D: ligand stimulated expression of CYP1A1 and CYP1B1 genes. E: LXRα. F: LXRβ binding assay using LanthaScreen TR-FRET coactivator kit (Thermo Fisher Scientific, Inc., Waltham, MA). Data represent means ± SE where *$p < 0.05$, **$p < 0.01$, ***$p < 0.001$ and ****$p < 0.0001$ at student *t*-test; #$p < 0.05$, ##$p < 0.01$, ###$p < 0.001$ and ####$p < 0.0001$ at one way ANOVA. For A (n ≥ 4), B (n = 3), C and D (n = 3), E and F (n = 4). Gene expression was measured after 8 h of keratinocytes treatment with secosteroids and presented as fold change vs ethanol (0.1%) control and with GADPH (C) and cyclophilin (D) serving as internal controls.

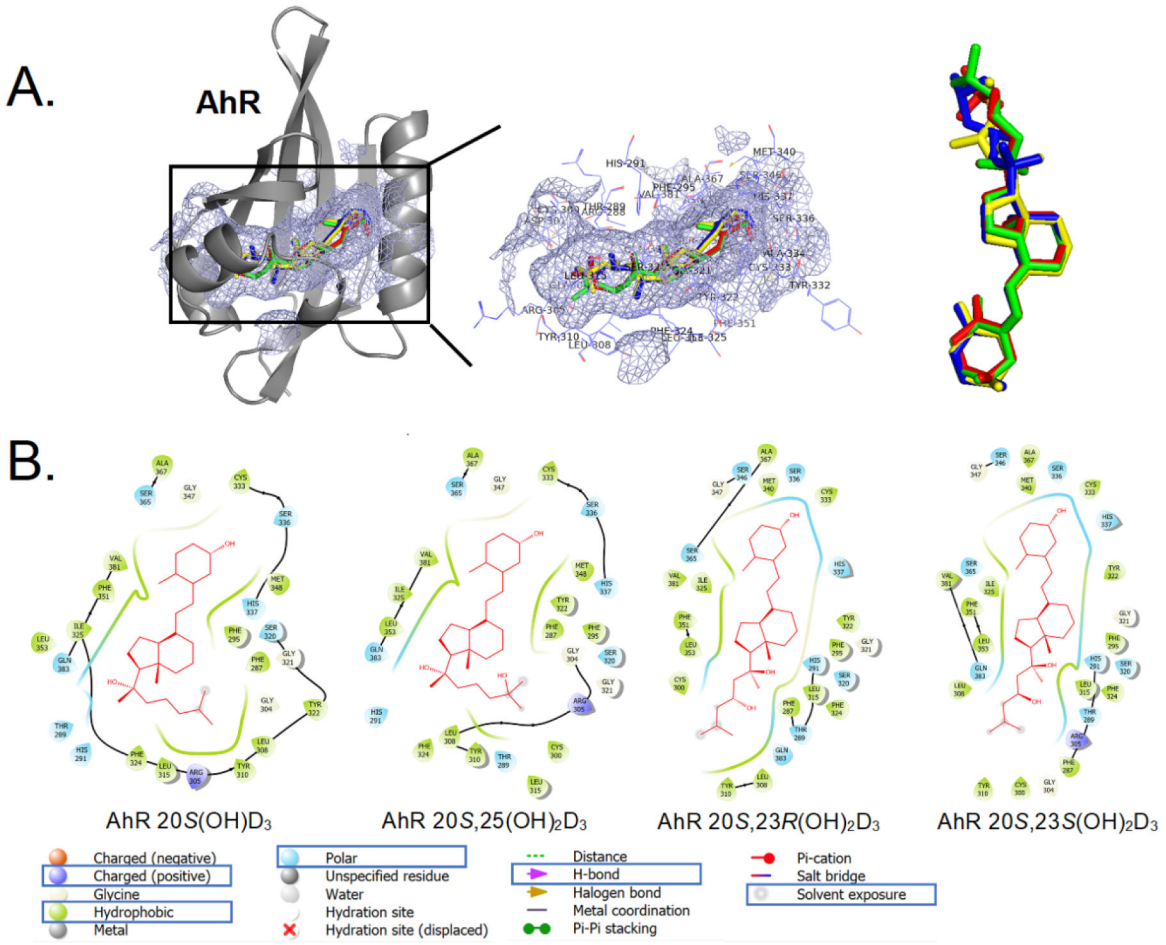

Figure 6a.

The binding pattern of selected vitamin D_3 derivatives with AhR. A: 3D binding modes for 20*S*(OH)D_3 (green), 20*S*,25(OH)$_2$$D_3$ (red), 20*S*,23*S*(OH)$_2$$D_3$ (blue) and 20*S*,23*R*(OH)$_2$$D_3$ (yellow) in ligand binding domain of AhR (cartoon in gray). The binding pocket is shown as a light blue meshing area. B: 2D interaction map of 20*S*(OH)D_3, 20*S*,25(OH)$_2$$D_3$, 20*S*,23*S*(OH)$_2$$D_3$ and 20*S*,23*R*(OH)$_2$$D_3$ with AhR (image generated with Maestro (v12.4)).

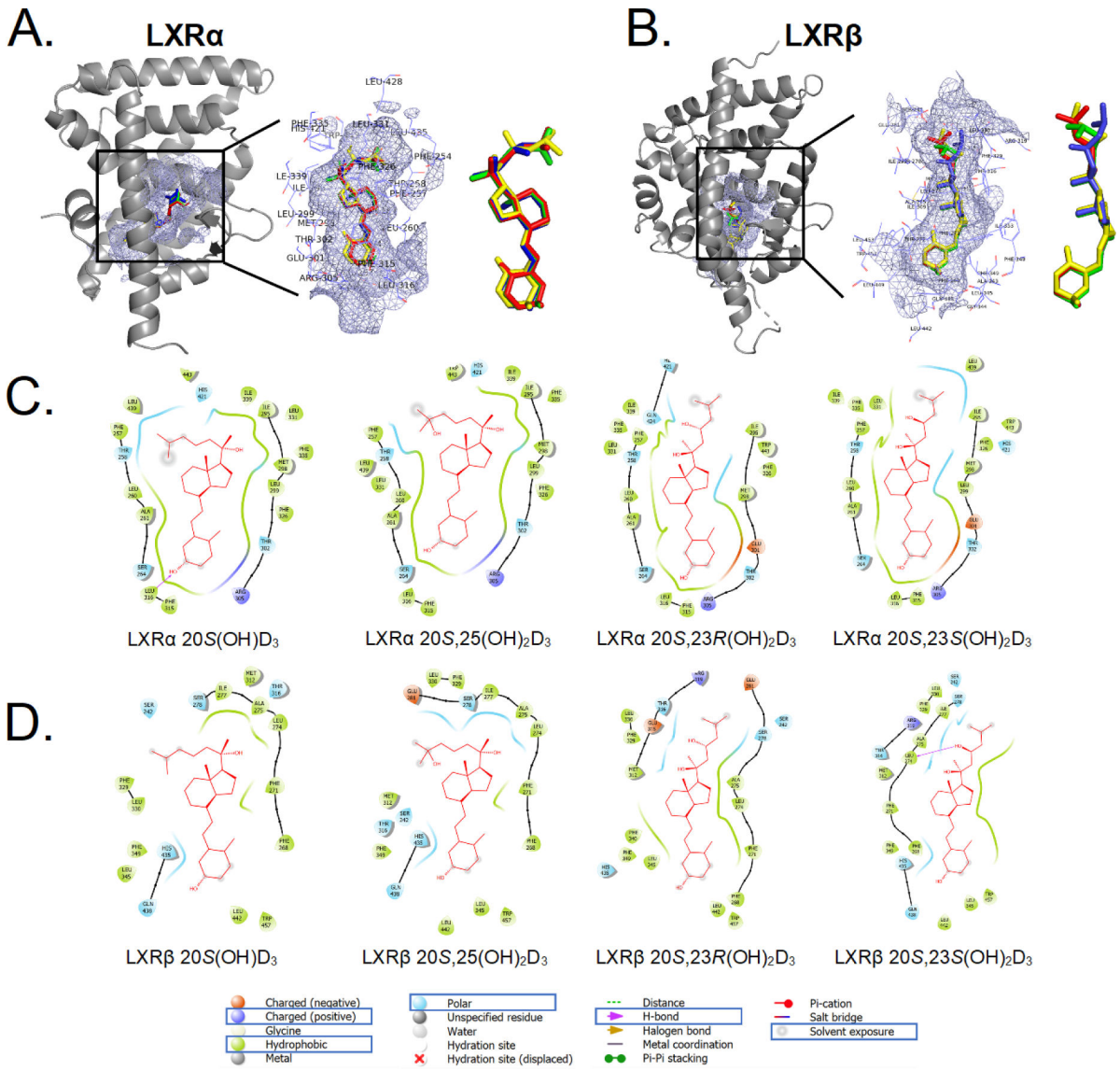

Figure 6b.

The binding pattern of selected vitamin D_3 derivatives with LXRs. A: 3D binding modes for 20*S*(OH)D_3 (green), 20*S*,25(OH)$_2$$D_3$ (red), 20*S*,23*S*(OH)$_2$$D_3$ (blue) and 20*S*,23*R*(OH)$_2$$D_3$ (yellow) in ligand binding domain of LXRα (cartoon in gray). B: 3D binding modes for 20*S*(OH)D_3 (green), 20*S*,25(OH)$_2$$D_3$ (red), 20*S*,23*S*(OH)$_2$$D_3$ (blue) and 20*S*,23*R*(OH)$_2$$D_3$ (yellow) in ligand binding domain of LXRβ (cartoon in gray) including a zoomed view. The binding pocket is shown as a light blue meshing area. C: 2D interaction map of 20*S*(OH)D_3, 20*S*,25(OH)$_2$$D_3$, 20*S*,23*S*(OH)$_2$$D_3$ and 20*S*,23*R*(OH)$_2$$D_3$ with LXRα. D: 2D interaction map of 20*S*(OH)D_3, 20*S*,25(OH)$_2$$D_3$, 20*S*,23*S*(OH)$_2$$D_3$ and 20*S*,23*R*(OH)$_2$$D_3$ with LXRβ (image generated with Maestro (v12.4)).

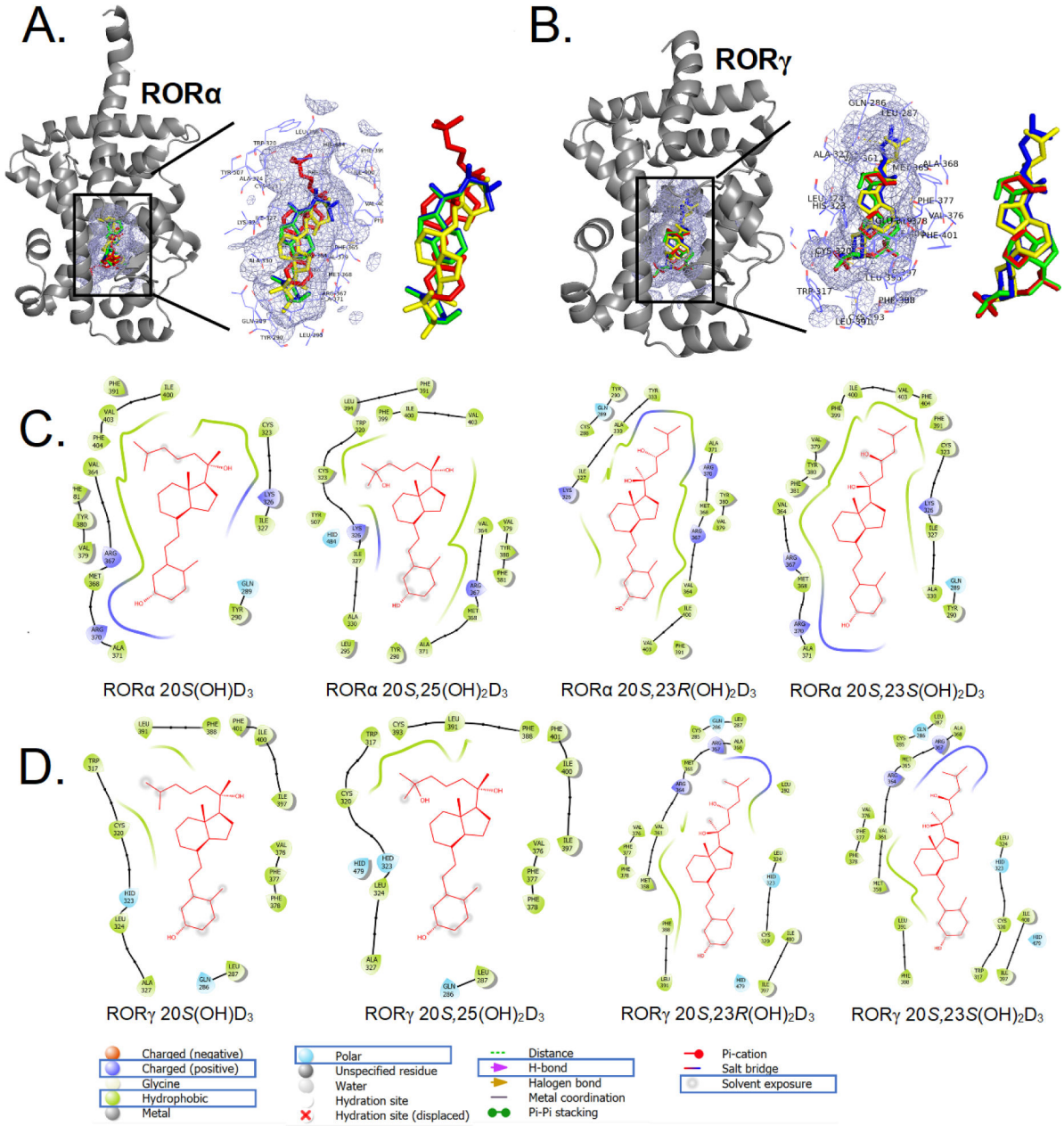

Figure 6c.

The binding pattern of selected vitamin D_3 derivatives with RORs. A: 3D binding modes for 20*S*(OH)D_3 (green), 20*S*,25(OH)$_2D_3$ (red), 20*S*,23*S*(OH)$_2D_3$ (blue) and 20*S*,23*R*(OH)$_2D_3$ (yellow) in ligand binding domain of RORα (cartoon in gray). B: 3D binding modes for 20*S*(OH)D_3 (green), 20*S*,25(OH)$_2D_3$ (red), 20*S*,23*S*(OH)$_2D_3$ (blue) and 20*S*,23*R*(OH)$_2D_3$ (yellow) in ligand binding domain of RORγ (cartoon in gray) including a zoomed view. The binding pocket is shown as a light blue meshing area. C: 2D interaction map of 20*S*(OH)D_3, 20*S*,25(OH)$_2D_3$, 20*S*,23*S*(OH)$_2D_3$ and 20*S*,23*R*(OH)$_2D_3$ with RORα. D: 2D interaction map of 20*S*(OH)D_3, 20*S*,25(OH)$_2D_3$, 20*S*,23*S*(OH)$_2D_3$ and 20*S*,23*R*(OH)$_2D_3$ with RORγ (image generated with Maestro (v12.4)).

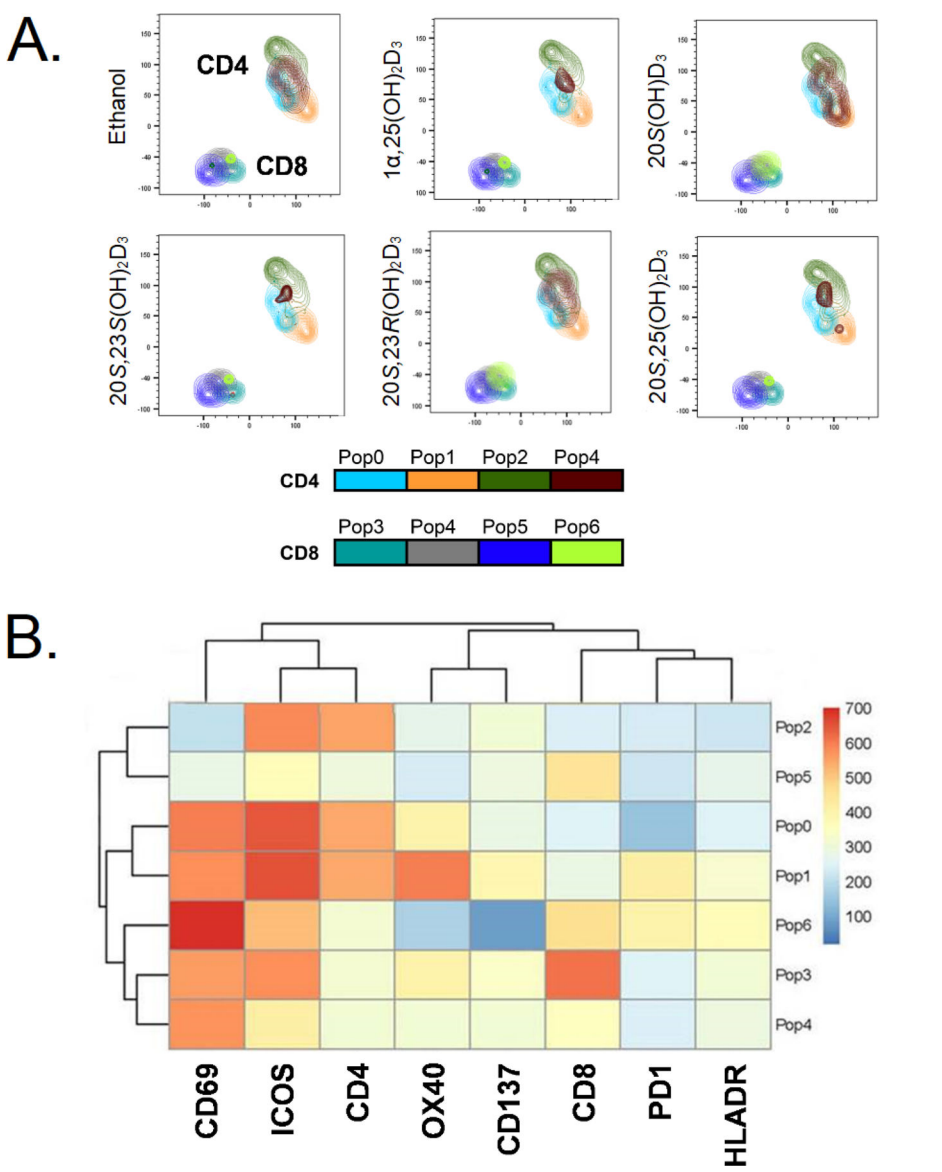

Figure 7.

Differential and overlapping effects of secosteroids on activation of CD4 and CD8 T cells from human peripheral blood. A: FlowSOM analysis shows that the different vitamin D_3 secosteroids variably alter CD4 and CD8 T cell activation. B: Heat map of FlowSOM clusters representing the level of expression of activation induced markers (AIM) on CD4 and CD8 T cell population shown in A. T cells in peripheral blood from two healthy individuals were activated with anti-CD3 and anti-CD28 in the absence (ethanol) or presence of 10^{-7} M of each of the vitamin D_3 secosteroids for 24 h. The cells were stained for lineage markers (CD4, CD8, CD19, CD14) and a panel of activation induced markers (CD69, ICOS, OX40, CD137, PD1, HLADR) and expression data were collected using a flow cytometer. The gating strategy was live, single cell followed by CD4 and CD8 T cell populations. The data file output following following CD4 and CD8 T cell gating from each individual were concatenated into one file and subjected first to the dimensionality reduction algorithm

TriMAP, which clusters cell populations based on relatedness using three points. The data shows that CD4 and CD8 T cell populations cluster independently as expected. Following TriMAP analysis, we performed clustering with Self-Organizing Maps (FlowSOM) and the identified clusters were overlayed on to TriMAP clusters. Pop0 to Pop6 are subpopulations of cells based on expression levels of all markers shown in the heat map (Fig. 6B). Unbiased analyses using TriMap dimensionality reduction clustering followed by FlowSOM “R” algorithm-based clustering defined these subpopulations based on the expression levels of the markers. The algorithm-based clustering analysis takes into consideration the expression levels CD4, CD8 and all AIMs. The expression levels for each marker in specific FlowSOM populations is output as a heat map B. The heat map reflects the levels of expression of each marker within each subpopulation (Pop0 – Pop6) and is not by itself reflective of response to a vitamin D3 analogue.

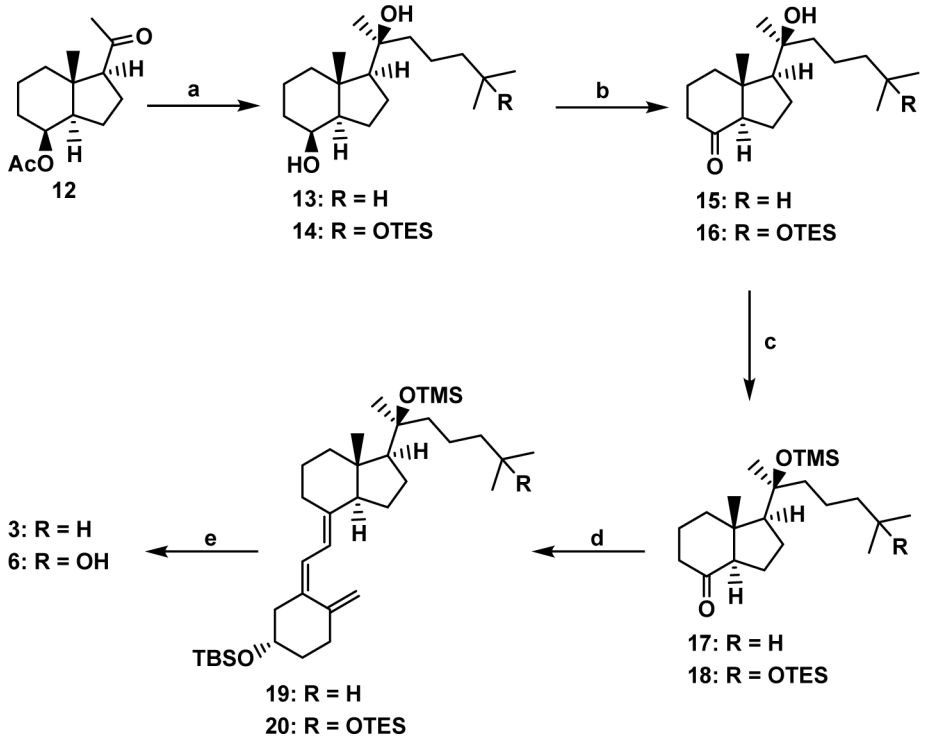

Scheme 1.

(a) for **13**: Mg, $Br(CH_2)_3CH(CH_3)_2$, THF, 0 °C → rt, 85%; for **14**: Mg, $Br(CH_2)_3C(CH_3)_2OTES$, THF, 0 °C → rt, 80%; (b) TPAP, NMO, 4 Å MS, CH_2Cl_2, 0 °C → rt, **15**: 77%, **16**: 80%; (c) TMSOTf, 2,6-lutidine, CH_2Cl_2, −78 °C, **17**: 84%, **18**: 82%; (d) **9**, *n*-BuLi, THF, −78 °C, **19**: 81%, **20**: 91%; (d) TBAF, THF, rt, **3**: 84%, **6**: 75%.

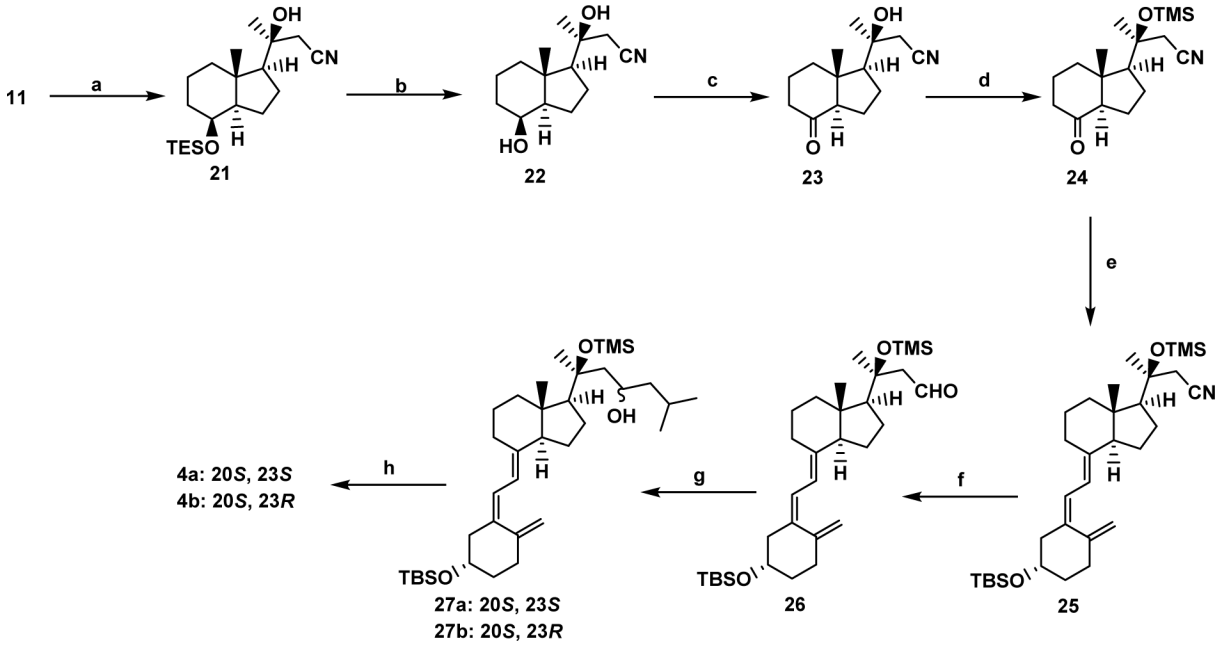

Scheme 2.

(a) CH_3CN, LDA, THF, −78 °C, 92%; (b) 4M HCl in dioxane, CH_2Cl_2, −78 °C, 98%; (c) TPAP, NMO, 4 Å MS, CH_2Cl_2, 0 °C → rt, 95%; (d) TMSOTf, pyridine, 0 °C, 74%; (e) **9**, *n*-BuLi, THF, −78 °C, 87%; (f) DIBAL-H, CH_2Cl_2, −78 °C, 62%; (g) *i*-BuMgCl, THF, 0 °C → rt, 70%; (h) TBAF, THF, rt, 74%.

Table 1.

Metabolism of chemically synthesized secosteroids by CYP27B1.[a]

Secosteroid	1α-hydroxylase activity (mol product/min/mol CYP27B1)
20*S*(OH)D_3	0.135 ± 0.005
20*S*,23*R*$(OH)_2D_3$	0.117 ± 0.027
20*S*,23*S*$(OH)_2D_3$	0.258 ± 0.020
20*S*,25$(OH)_2D_3$	7.98 ± 0.24

[a]Secosteroids were incorporated into phospholipid vesicles at a ratio of 0.025 mol secosteroid/mol phospholipid and incubated with mouse CYP27B1 (0.2 μM) for 20 min for all substrates except 20*S*,25$(OH)_2D_3$ which was incubated for 5 min. Extracted samples were analyzed by reverse-phase HPLC. Data are mean ± SD, n=3.

Table 2.

Molecular docking results for the complexes of vitamin D_3 hydroxy derivatives with selected nuclear receptors (kcal/mol).

Secosteroid \ Nuclear Receptor		VDR	RORα	RORγ	LXRα	LXRβ	AhR
Control	20(OH) Cholesterol	N/A	−11.4	−10.7	−10.0	−9.2	N/A
	25(OH) Cholesterol	N/A	−11.5	−10.9	−9.8	−9.8	N/A
	Indole acetic acid	N/A	N/A	N/A	N/A	N/A	−8.0
	1α,25(OH)$_2$D$_3$	−11.8	−11.3	−10.7	−10.9	−11.0	−12.0
20*S*(OH)D$_3$		−11.6	−10.7	−10.2	−10.2	−11.0	−11.9
20*S*,25(OH)$_2$D$_3$		−11.9	−10.8	−10.1	−10.2	−11.0	−11.6
20*S*,23*S*(OH)$_2$D$_3$		−11.4	−10.7	−10.1	−10.0	−11.1	−11.9
20*S*,23*R*(OH)$_2$D$_3$		−11.6	−10.7	−10.3	−9.9	−10.5	−11.8